1976

X-ray diagnostics of laser-produced aluminum plasmas.

Shewchuk, Sydney A.

Monterey, California. Naval Postgraduate School

X-RAY DIAGNOSTICS OF LASER-PRODUCED ALUMINUM PLASMAS

Sydney A. Shewchuk

NAVAL POSTGRADUATE SCHOOL
Monterey, California

THESIS

X-Ray Diagnostics of Laser-Produced Aluminum Plasmas

by

Sydney A. Shewchuk

Thesis Advisor: A.W. Cooper

Approved for public release; distribution unlimited.

UNCLASSIFIED

SECURITY CLASSIFICATION OF THIS PAGE *(When Data Entered)*

REPORT DOCUMENTATION PAGE

READ INSTRUCTIONS BEFORE COMPLETING FORM

1. REPORT NUMBER

2. GOVT ACCESSION NO.

3. RECIPIENT'S CATALOG NUMBER

4. TITLE *(and Subtitle)*

X-Ray Diagnostics of Laser-Produced Aluminum Plasmas

5. TYPE OF REPORT & PERIOD COVERED

Masters Thesis; June 1976

6. PERFORMING ORG. REPORT NUMBER

7. AUTHOR*(s)*

Sydney A. Shewchuk

8. CONTRACT OR GRANT NUMBER*(s)*

9. PERFORMING ORGANIZATION NAME AND ADDRESS

Naval Postgraduate School
Monterey, California 93940

10. PROGRAM ELEMENT, PROJECT, TASK AREA & WORK UNIT NUMBERS

11. CONTROLLING OFFICE NAME AND ADDRESS

Naval Postgraduate School
Monterey, California 93940

12. REPORT DATE

June 1976

13. NUMBER OF PAGES

125

14. MONITORING AGENCY NAME & ADDRESS*(if different from Controlling Office)*

15. SECURITY CLASS. *(of this report)*

UNCLASSIFIED

15a. DECLASSIFICATION/DOWNGRADING SCHEDULE

16. DISTRIBUTION STATEMENT *(of this Report)*

Approved for public release; distribution unlimited

17. DISTRIBUTION STATEMENT *(of the abstract entered in Block 20, if different from Report)*

18. SUPPLEMENTARY NOTES

19. KEY WORDS *(Continue on reverse side if necessary and identify by block number)*

X-ray diagnostics
Plasma temperature
Neodymium laser
Laser-Produced Aluminum plasma
PIN diode x-ray detector
Vacuum photodiode

20. ABSTRACT *(Continue on reverse side if necessary and identify by block number)*

Electron temperatures have been evaluated using the x-ray emission from plasmas created by irradiating a solid Aluminum target with a 500MW, 25nsec Nd laser. Studies of the x-ray emission from the plasma at $5 \times 10^{11} W/cm^2$ using the two foil absorption method indicated temperatures ranging from 136 to 185eV. No suprathermal activity was detected for the foil combinations used. Temperature was related to

DD FORM 1 JAN 73 1473 EDITION OF 1 NOV 65 IS OBSOLETE
S/N 0102-014-6601 |
(Page 1)

UNCLASSIFIED

SECURITY CLASSIFICATION OF THIS PAGE *(When Data Entered)*

laser flux density by the scaling factor 0.404. Observed temperature remained constant for cratering with up to 25 laser pulses focused at the same spot. Preliminary measurements indicated x-ray intensity was proportional to $P^{\frac{1}{4}}$ over the range 10 to 300 microns.

Initial work was completed on a vacuum photodiode useful for high resolution photon detection in the soft x-ray region of the spectrum.

X-Ray Diagnostics of Laser-Produced Aluminum Plasmas

by

Sydney A. Shewchuk
Captain, Canadian Armed Forces
B.Sc. Chem. Eng., University of Alberta, 1968

Submitted in partial fulfillment of the
requirements for the degree of

MASTER OF SCIENCE IN PHYSICS

from the
NAVAL POSTGRADUATE SCHOOL
June 1976

ABSTRACT

Electron temperatures have been evaluated using the x-ray emission from plasmas created by irradiating a solid Aluminum target with a 500MW, 25nsec Nd laser. Studies of the x-ray emission from the plasma at 5×10^{11} W/cm^2 using the two foil absorption method indicated temperatures ranging from 136 to 185eV. No suprathermal activity was detected for the foil combinations used. Temperature was related to laser flux density by the scaling factor 0.404. Observed temperature remained constant for cratering with up to 25 laser pulses focused at the same spot. Preliminary measurements indicated x-ray intensity was proportional to $P^{1/4}$ over the range 10 to 300 microns.

Initial work was completed on a vacuum photodiode useful for high resolution photon detection in the soft x-ray region of the spectrum.

TABLE OF CONTENTS

LIST OF TABLES

LIST OF FIGURES

ACKNOWLEDGEMENT

I would like to acknowledge the valuable technical assistance of Bob Sanders and his colleagues whose response to requests for technical aid and whose cooperative attitudes in times of stress helped make this project a success.

Appreciation is extended to foreman Pete Whistler of the NPS Machine Facility for the priority given to my work and to master machinist Frank Abbe for turning rather poor sketches into superb plasma diagnostic equipment.

Special thanks is directed to Professors Cooper, Schwirzke, Dally, and Buskirk for their concern, patience, and willingness to provide help whenever called upon.

This study was sponsored by the Office of Naval Research.

I. INTRODUCTION

Continued improvements in the energy output and control of pulsed laser systems has stimulated intensive theoretical and experimental interest in their use for the production and study of hot, dense microplasmas. Of the many areas of research involving hot plasmas, the best known is the possibility of achieving controlled thermonuclear fusion by means of laser heated plasmas. The temporal and spectral emission distribution of soft x-rays from such plasmas, while constituting an energy loss mechanism in fusion-type experiments, can be used as a powerful tool in the study of plasma electron temperature, energy distribution of electrons and the development and origin of various instabilities. Fusion studies are directed towards laser heating of low nuclear charge(Z) fusionable materials. By using high Z materials such as Aluminum, the emitted x-rays become a source for irradiation and for determination of energetic atomic levels.

When a laser pulse of sufficient energy density and duration ($>10^{9}$ W/cm^{2})[1] strikes a solid opaque target, laser light is absorbed and blowoff material is removed from the target surface. The material removed consists of both neutral particles and charged particles (electrons and ions) which, when considered as a dense cloud of quasi-neutral interacting ionized gas, is defined as a plasma. Further heating takes place by absorption of laser light in the expanding plasma. This is accomplished through several processes including the inverse Bremsstrahlung process which involves absorption of a photon by a free electron which is raised to a higher state in the continuum available to it. In this way plasmas can be readily heated to temperatures in

excess of 10^7 °K which corresponds to approximately 100eV by the relation, 1eV = 11,600°K.

Much of the energy which has been absorbed by the plasma via the mechanisms of ionization and heating, production of fast particle groups and intense magnetic field generation must subsequently be emitted as the laser plasma expands. A limited portion of the incident energy (usually <15%) is emitted in the form of continuum radiation and the characteristic spectral lines of the target element's highly ionized states. Most of the radiant energy has short wavelength (<100Å) placing it in the loosely defined soft x-ray range, and the average energy of the photons corresponds roughly to the electron energy[2].

The continuum portion of the x-ray emission is a very useful tool, when coupled with foil absorption theory, for determination of plasma temperatures and anomalous heating effects. The dependence of high-energy cutoff on temperature allows determination of the high-energy continuum wavelength distribution and hence, a rather sensitive measurement of the plasma electron temperature. The diagnostic techniques involved in the deconvolution of plasma temperatures from x-ray emission will be the topic of most of the discussion in following sections.

This study is the initial phase of an NPS Plasma Physics program to establish a plasma x-ray diagnostic facility capable of studying electron temperature behavior particularly in the area of anomolous electron heating. More specifically, it encompasses the design, manufacture, calibration and implementation of x-ray detection equipment which can subsequently be employed in detailed studies of early plasma temperature characteristics. In addition to assembly of experimental hardware, this report contains a

summary of previous efforts in this area of research and a detailed description of how temperature data is extracted from x-ray information.

II. PREVIOUS WORK

X-ray emission from a plasma was first observed in 1930 by several research teams[3], but the first attempt to put the discovery to use in the evaluation of plasma parameters such as density and temperature was not until 1936[4]. X-ray experimentation was restricted, however, by weak, low temperature spectra contaminated by impurities. These conditions existed until the early 1960's when the advent of high power short pulse lasers provided a convenient source for vacuum ultraviolet and soft x-radiation by irradiation of targets. Much of the ensuing research in the field has been devoted to improving x-ray emission quality and quantity, refining diagnostic techniques to obtain accurate plasma temperature evaluations and discovering the existence and origin of instabilities.

Two such early studies, unrelated to laser work, are considered the foundation of much of current developments. The first is a paper by Jahoda[5] in 1960 concerning the continuum radiation in the x-ray and visible regions from a Theta-Pinch (Scylla) plasma. This was the first electron temperature measurement using the two foil absorption technique. This technique involves measurements of the continuum radiation passing through broadband filters constructed from thin metallic foils. A comparison of the intensities transmitted through foils of various materials and various thicknesses determines the wavelength distribution of the continuum intensity and, thereby, the electron temperature. Considerable data was compiled relating to the x-ray absorption characteristics of Beryllium(Be), Aluminum(Al), Nickel(Ni) and Carbon(C) whose mass absorption coefficients as functions of wavelength are shown in Figure 1. These absorption measurements yielded

information about the spectrum of incident x-rays by the shape of the plot of transmitted intensity versus absorber thickness. The techniques and data continue to be of use to present day experimentalists.

The second significant accomplishment came in the form of two Naval Research Laboratory (NRL) reports by Elton[6,7]. These reports presented the calculations of the wavelength distribution of Bremsstrahlung continuum radiation per unit wavelength interval in the soft x-ray spectral region transmitted through various metallic filters. Also calculated were the total integrated Bremsstrahlung radiation passing through absorbing foils of Be, Al, Ni and C (and foil combinations) for temperatures varying from 50 eV to 100keV. This information is vital in obtaining values for the electron temperature in a plasma from measurements of the soft x-ray continuum emission.

The foil absorption technique is still the most widely used in temperature determination, but an extension of it called the Ross Filter was suggested by Van Paassen[8] in 1971 for Z-pinch devices and by Bernstein[9] in 1972 for plasma focus devices. The Ross filter is ideally suited to plasma devices which exhibit random variations in intensity, spatial distributions and spectral shape from pulse to pulse. It consists of two identical detectors placed behind two x-ray absorbing foils made from adjacent elements on the periodic chart. Thicknesses of the foils are adjusted to achieve matched transmission for all x-ray energies except the range between the K edges. This produces an experimental x-ray spectrum directly and avoids having to fit transmission measurements with theoretical transmission values for an assumed model. The highest K-edge available is that of Uranium at 116 KeV, which places an upper limit on the energy range for the Ross filter system. Lower limits are determined by the difficulty in making uniform

foils of filter elements that will transmit measureable amounts of x-radiation. Johnson[10] designed a 15 channel Ross filter system which considerably reduced data reduction time and produced a ten point energy spectrum ranging from 4.5 to 116keV for each x-ray pulse.

Much of the early study of laser plasma electron temperatures was directed towards confirmation that reasonably accurate temperatures could indeed be estimated from x-ray intensity emission. Targets for the laser pulses were low Z materials such as Deuterium and Lithium which were used in nuclear fusion research. X-ray intensities were detected by scintillator-photomultiplier combinations placed behind metal absorption filters. This form of detection allows good time resolution (<10nsec) when x-ray intensities are large. Response of the scintillator is linear over a wide wavelength range whose lower limit is approximately 8Å. Output of the photomultiplier is directly proportional to the x-ray flux passing through the metal foil.

One of the first extensions of the x-ray temperature measuring technique was to demonstrate the relationship between electron temperature and laser power incident on the target, ϕ. Early models based on a one dimensional flow approximation involved the laser pulse duration, t, as shown in relation 1,

$$T_e \propto \phi^{1/2} t^{1/4} \qquad (1)$$

This model is non-stationary in that temperature increases with time as the plasma flows towards the incoming laser light. It is unrealistic for long duration pulses because of the radial expansion of the plasma and subsequent decrease of absorptivity.

A more acceptable model was proposed by Bobin[11] and others, for steady state situations where the laser pulse duration is longer than the heating time of the plasma (heating time is of the order of r/v where r is focal spot size and v is thermal flow velocity). The resulting scaling law is shown in relation 2,

$$T_e \propto \phi^{4/9} r^{2/9} \qquad (2)$$

where the constant of proportionality depends on the plasma absorption coefficient.

A simple limiting case of relation 2 assumes that heating is localized to a plane of critical density and the calculated plasma temperature is independent of assumptions about the flow geometry. T_e becomes dependent on the two thirds power of laser flux density which is useful in showing the general distribution of energy in the spectrum.

When it became apparent that laser x-ray spectroscopy had established itself as a reliable diagnostic method for fusion research, higher Z materials were substituted for the traditional Deuterium and Lithium. The new materials such as Aluminum, Magnesium and Iron had a much higher x-ray flux density and offered the unique advantage that the ionization stages produced by the laser beam were already a reasonably good indicator of the electron temperatures reached in the plasma. This spurred interest in laser-energy to x-ray conversion efficiency led to a paper by Mallozzi[12] describing laser-generated plasmas as a source of x-rays for medical applications. In an effort to produce high resolution medical radiographs, x-ray conversion efficiencies of greater than 25% were reported for Nd laser light focused onto solid iron and copper targets. The

technique was to vaporize and ionize material near the focal spot by a prepulse (1J, 10nsec, 10^{11} W/cm^2) and heat the resulting plasma by a main pulse (100J, 10nsec, 10^{14} W/cm^2) via the inverse Bremsstrahlung absorption process. For medical radiographs of thin samples, the x-rays in the vicinity of 1keV, which comprise the bulk of the emitted spectrum, would be employed. For thicker samples to be studied, the harder (though sparser) 2 to 20keV range would be useful. The laser source with its short pulse width would match the resolution of conventional sources while having the unique capability of arresting biological motion that might occur with living samples being photographed. Conversion efficiencies in excess of 50% have been shown to be theoretically possible if the plasma can convert a significant fraction of laser energy to x-rays in less than 1nsec so that little energy will be available to generate strong magnetohydrodynamic motion[13]. Mallozzi's experiment was significant in the field of plasma temperature diagnostics in that he developed an x-ray pipe, similar to a light pipe, capable of channelling soft x-rays to internal locations of the body without damaging intervening tissue. The device enhanced x-radiation delivered on a line-of-sight path by a factor of 32. Curved tube enhancement was about 8 times. These experiments lead to a class of x-ray pipe devices for enhancing the deposition of plasma radiation on photographic film. Of particular interest is an experiment by Lieber[14] who has used micro-channel plate(MCP) for collimating soft x-ray images emitted by laser plasmas, thus significantly increasing spatial resolution. While the extremely simple pinhole camera is still the most popular for spatial resolution, collimating devices are gaining in popularity especially in areas where x-ray flux densities are very

limited by laser, target or environmental considerations.

Solid state detectors for temporal resolution came into use with the foss filter systems[8,10] because of their fast response time, low voltage requirements and ease of situating large numbers of detectors in confined spaces. The silicon surface barrier detector and the diffused junction detector are available for x-ray detection with the latter silicon PIN diode being the most popular because of its greater sensitivity to high energy x-ray photons (>1 keV). PIN diodes consist of an entrance window dead layer of 0.3 to 1.0 microns(N), an active(depletion) layer of 75 to 500 microns(I) and a positive silicon layer(P). Upper and lower energy detection limitations are determined by the thicknesses of the active layer and dead layer respectively. For production of one electron-hole pair in silicon an energy of only 3.6 eV is needed so that a linear response can be expected in the soft x-ray region[15]. Surface barrier detectors ought to be more sensitive to low energy x-rays than PIN diodes because of their negligible dead layers. However, even the thinnest K-edge absorption filters are too thick to allow exploitation of this potential advantage.

X-ray diagnostics could be very useful in the study of laser compression fusion, where the time response of plasma parameters to shaped laser pulses has a subnanosecond resolution scale, if a suitable detector were available. Key[16] constructed such a detector in the form of an x-ray vacuum photodiode capable of a resolution of 1.0nsec compared to scintillator-photomultiplier or semiconductor diode resolution times of 2 to 5nsec. The vacuum diode was cylindrical with a central anode biased at 3000V surrounded by a cathode and the intervening space evacuated to chamber pressure (10^{-5} Torr). One end of the cylindrical structure

was covered with the absorption foil while the signal and high voltage leads were connected to the other end. Several layers of RF screen and insulation completed the superstructure. The diode had an absolute quantum efficiency of 30% and a response time of 1.0nsec. Following the basic design cited by Key, a similar type diode will be constructed as part of the NPS diagnostic program.

Assuming a Maxwellian velocity distribution, radiation from a plasma is thermal in nature resulting from Bremsstrahlung and recombination. There is, however, a peculiarity of plasma x-radiation demonstrated by the phenomenon of suprathermal electrons which creates abnormal spikes in the x-ray emission spectrum[17]. The non-thermal radiation from a plasma brought about by these fast electrons causes deviation from electron temperatures calculated under the assumption of a Maxwellian velocity distribution. Figure 2 shows the x-ray intensities passing through Beryllium and Aluminum foils of different thicknesses. The two solid lines indicate temperatures of 2keV and 0.5keV calculated by assuming a Maxwellian distribution. They are straight lines on a semi-log plot with a negative slope as predicted by theory. The curve of measured values indicates, not a single temperature, but temperatures varying from 500eV to approximately 2keV (extrapolated to an extreme point on the graph). This means that the x-ray emission is enhanced up to a factor of 10^5 at the high energy end of the measured interval (15keV). If the laser energy is lower, the calculated curve is shifted to the left and long wavelength x-radiation can no longer penetrate the thinnest foils. The enhancement effect then dominates the entire measuring range and simulates too high temperatures[18]. Thus anomalous temperatures from x-ray measurements can be used as an indication of the existence

of suprathermal electrons.

Suprathermal electrons were noticed in experiments as early as 1968[19] and have been attributed to several possible causes including growing-mode or oscillating two stream instability[20], core-corona decoupling[21] and parametric interaction between plasma and light (parametric ion-acoustic instabilities)[17,18,22-24]. Although the mechanism for production of suprathermal electrons is not fully understood, it is widely believed that the cause originates in the ion-acoustic instability.

The ion-acoustic instability is initiated as ions form a uniform background for electrons oscillating coherently and colliding in the local light field. As the electron and ion fluids are heated, they begin to oscillate independently in the absence of external fields. Ions oscillate at the ion-acoustic frequency and electrons oscillate at the electron plasma frequency. The strong electromagnetic field of the laser beam couples the two oscillations by means of the space charges which are created. In the neighborhood of the plasma frequency, ion and electron fluctuations of suitable wavelengths may be driven unstable. This results in the distortion of the Maxwellian electron distribution and the generation of groups of fast particles (suprathermal electrons). The energy of the unstable waves is then converted into thermal energy by collisional and Landau damping[18].

Nishikawa[19] established the basic formulation for determining the onset of parametric instabilities. He was able to derive simple model equations for the coupling of two waves due to the presence of a third wave with large amplitude. When certain plasma parameters are known, the equations are able to predict an approximate value for the power density necessary to perturb the plasma to an unstable

condition. For a Nd laser with plasma density 10^{21} cm^{-3}, and electron temperature 150eV, the threshold laser power density is approximately 1.5×10^{13} W/cm^2.

At the NPS Plasma Physics facility, McKee[25], determined theoretically the relationship between laser flux and plasma temperature by using a computer code to solve numerically equations 4.49 and 4.51 of reference 1 for irradiation of a 5 mil thick mylar foil with a 300MW, 25nsec full width at half maximum (FWHM) Nd laser pulse. The maximum temperature obtained was approximately 100eV which occurred several nanoseconds after arrival of the maximum laser intensity at the target. The model used did not include the effects of background pressure which influences the plasma expansion dynamics. This is a result of incident laser energy ionizing the ambient gas background creating a plasma-plasma interaction.

A continuation of McKee's work by Bird[26] with an emphasis on expansion of the plasma into various background pressures showed the development of reverse magnetic fields attributed to the creation of an axial electron temperature gradient at the plasma front due to snowplowing of the ambient plasma. The magnetic field was predicted to scale as the cube root of the ambient plasma density.

An attempt will be made in this study to experimentally confirm the maximum temperature/laser pulse relationship predicted by McKee and to determine the scaling relation that exists between the ambient background pressure and the x-ray intensity emitted from the plasma.

III. THEORY

A. LASER ENERGY ABSORPTION

An intense laser light pulse incident on a target couples with the target material. If the target is sufficiently opaque then it can be assumed there is no transmission. All of the energy is either absorbed or reflected where reflection is initially governed by optical reflectivity. Absorption occurs through a coupling of light with the target material. Photon energy is converted into thermal and mechanical energy and the plasma is initiated.

Free electrons are initially produced by an as yet unknown mechanism. Since the laser light photon energy ($h\nu$=1.17eV for Nd laser) is less than the ionization energy of the atoms (5.98eV for Al^{+}), direct photoionization cannot occur and other possible mechanisms have been suggested: multiphoton ionization (absorption of 6 photons in this case), stimulated Raman effect, easily ionized impurities, surface effects, or ionization due to scattered ultraviolet light from the laser flash lamps. The absorption process is thus divided into two stages, the production of the initial ionization and the subsequent cascade by which the ionization grows. The avalanche process in which a single light quantum is absorbed by a free electron in the field of a heavy ion or atom (to conserve momentum) is called inverse Bremsstrahlung. This is equivalent to the resistive damping of the laser light wave due to electron-ion collisions[27]. The free electrons with increased energy ionize other atoms and the target surface at the focal spot is rapidly transformed into an ionized absorbing plasma even in the initial stages of interaction when a negligible amount of the pulse energy has been delivered.

Energy flux is absorbed in the plasma over a distance L in accordance with the equation

$$W = W_0\{1-\exp(-\kappa L)\} \qquad (3)$$

where W_0 is the incident laser energy flux and κ in inverse centimeters is the absorption coefficient given by[1]

$$\kappa = 3.69\times10^{-8}\,(Z^3 n_i^2/T_e^{1/2}\nu^3)\{1-\exp(-h\nu/kT_e)\} \qquad (4)$$

n_i and n_e are ion and electron densities in cm^{-3} in a plasma of average charge Z and temperature T_e in electron volts, ν is the laser frequency, c is the velocity of light, e is electronic charge, m is electron mass, h is Planck's constant and k is Boltzmann's constant. The term

$$1-\exp(-h\nu/kT_e)$$

accounts for losses by stimulated emission.

If the plasma frequency is close to the laser light frequency then the classical absorption length of a plasma is

$$L = 5\times10^{18}\,T^{3/2}/n_e \qquad (5)$$

where L is in microns. For a plasma temperature of 100eV and density 10^{20} cm^{-3}, L is 50 microns. Efficient heating

requires that the plasma absorbs light throughout its characteristic dimension, L_p. If L is greater than L_p then the plasma becomes transparent to a portion of the incident laser light and energy will be lost; if L is much less than L_p then energy is dumped mostly at the surface and the plasma will not be heated uniformly.

Laser radiation cannot propagate at plasma densities higher than the critical density defined as

$$n_c = m\omega^2/4\pi e^2 \qquad (6)$$

where the optical frequency ω must be greater than the plasma frequency ω_p. For the Nd laser (λ=1.06μm) the critcal density of the plasma is 10^{21} cm^{-3}. Concentrations of free electrons beyond this density will cause reflections of incident light. It is, however, desirable to have a layer of electron density as close as possible to n_c in order to maximize the absorption coefficient .

Absorbed energy goes primarily into electron kinetic energy. The time for equilibration transfer of absorbed energy from electrons to ions is of the order[1]

$$t \approx 252AT_e^{3/2}/n_e Z^2 \ln \Lambda \qquad (7)$$

where T_e is in °K and n_e is in cm^{-3}. $\ln\Lambda$ is approximately 10 for a wide range of plasma parameters and A is the atomic weight of the ions. For an Aluminum plasma (A=27, Z=3) of temperature 10eV ($T=1.16\times10^6$ °K) and density 10^{20} cm^{-3}, equilibration time is

$$t_e \approx 10^{-12} \text{ seconds}$$

The duration of the Nd laser pulse is approximately 50nsec with a FWHM of 25nsec. The plasma, therefore, is heated during the laser pulse of approximately

$$t_p \approx 5\times10^{-8} \text{ seconds}$$

and the time for an electron to relax to the equilibrium Maxwellian distribution is short ($t_e << t_p$). Thus the plasma temperature and electron temperature are approximately equal and most of the properties of the absorption and emission can be described by the parameter T_e, the electron kinetic temperature. For pulses approaching picosecond duration the electron-ion energy transfer process cannot be regarded as instantaneous.

Plasma motion after the initial photoionization can be described by a hydrodynamic flow in which mass, energy and momentum are conserved. The various zones of interaction illustrated in Figure 3 are: (1) is the laser light absorption zone with density of the rapidly expanding plasma

cloud increasing towards the highly absorbing slab at F where electron density equals the critical density. New material is ionized at F to sustain the plasma. (2) is the zone where the plasma density is that of the shock compressed solid and heating is by heat conduction. The pressure at F initiates a compression wave which travels with its shock front S into the target to conserve momentum. (3) is the undisturbed solid.

Free electrons in a Maxwellian velocity distribution lose their energy by inelastic collisions with ions, X, of positive charge, z, via ionization and excitation,

$$e + X_z \longrightarrow e + e + X_{z+1} \quad \text{(ionization)} \tag{8}$$

$$e + X_z \longrightarrow e + X_z^* \quad \text{(excitation)} \tag{9}$$

and by the radiation processes: Bremsstrahlung, recombination and line transitions.

$$e + X_z \longrightarrow e + X_z + h\nu \quad \text{(Bremsstrahlung)} \tag{10}$$

$$e + X_{z+1} \longrightarrow X_z + h\nu \quad \text{(recombination)} \tag{11}$$

$$X_z^* \longrightarrow X_z + h\nu \quad \text{(line)} \tag{12}$$

The inverses of these are inverse Bremstrahlung, photoionization and photo-excitation[28]. Consideration of the three radiative processes shall be the topic of the next section.

B. PLASMA X-RAY EMISSION

Energy which has been absorbed by a target must be converted to new forms or emitted as electromagnetic radiation so that conservation laws will apply. Radiation from the plasma is both continuum and line, and when the plasma energy is high enough, wavelengths of interest fall in the x-ray region. The term x-ray, as used here, refers to the electromagnetic spectral region where wavelengths are less than 100Å. Soft x-rays with low penetrative power fall in the approximate region 100Å to 1Å. From Figure 4 this can be converted to the energy band of about 100eV to 10keV.

X-rays generated in high-energy laser plasmas have the usual Bremsstrahlung and recombination continua of ionized gases at lower energies and line emission similar to the type usually viewed in the optical spectrum. Examination of the radiative processes in the x-ray region is therefore not a new spectroscopic technique. It is merely an extension of well known methods into a high energy region of the spectrum in order to determine plasma properties.

The extension of diagnostics for high temperature plasmas into the x-ray region is essential for obtaining complete spectroscopic information. This is made apparant by considering the wavelength of the maximum in the intensity distribution of a Black-Body radiator. This is related to temperature by Wien's displacement law

$$\lambda_m T = 0.29 \text{ [cm } ^\circ\text{K]} \tag{13}$$

At temperatures of 10^5, 10^6 and 10^7 °K, the radiation spectral intensity maximum appears at 290, 29 and 2.9Å, clearly within the defined soft x-ray region for

temperatures greater than 10^6 °K. The black-body theory is an incorrect assumption for a plasma since it will radiate in this manner only for frequencies at which the absorption length is less than the plasma dimensions[1]. The rate of radiation would obey the Stefan-Boltzmann law

$$E = \sigma T^4 \quad [W/cm^2] \tag{14}$$

where σ is the Stefan-Boltzmann constant (5.67×10^{-12} $W/cm^2\ °K^4$). At a temperature of 10^7 °K, E is 5.67×10^{16} W/cm^2 which is a much larger amount of energy than the plasma can support. Radiation intensities from a plasma are much less than this for the temperature indicated (i.e. less than the incident laser energy density) but the Black-body theory is useful in indicating the approximate spectral location of the peak intensity regardless of its magnitude. It applies to the optically thick situation where radiation from the interior does not get out. A better radiation model would be a Grey Body distribution for which the emissivity is much less than one while the distribution retains the characteristic Black Body shape. This model is valid for an absorption length greater than or comparable with the plasma characteristic length.

Line radiation in a plasma occurs for electron transitions between discrete or bound energy levels of multiply charged ions from heavier elements. Lighter elements such as Hydrogen and Helium are usually completely stripped in a high temperature plasma resulting in no line radiation. Intensity of line radiation from highly ionized atoms in an optically thin plasma is

$$I_L = (4\pi)^{-1} A_{kn} h n_{zn} \delta \qquad (15)$$

where A_{kn} is the transition probability, n_{zn} is the ion density in quantum level n and δ is the thickness of the optical layer. If a Boltzmann distribution could be assumed between upper and lower states, the ion density could be easily calculated and an accurate value for I_L would result. This is not the case, however, since thermal equilibrium rarely exists between the ground state and the excited state. A rough calculation of line intensity can be achieved by assuming that transitions from lower states dominate the radiation and by applying approximate ion cross sections. Summation over all transitions can be omitted if it is further assumed that most radiation occurs in the resonance line, leaving the relation,

$$I_L \propto n_{z^1} n_e (E_e)^{3/2} (kT_e)^{-1/2} \exp(-E_{n^1}/kT_e) \qquad (16)$$

where E_{n^1} is the excitation of the resonance line. Temperature diagnostics becomes difficult at this point because of the interdependence of density and electron temperature. A further complication is broadening of resonance peaks by Doppler and collision mechanisms.

The ultimate result of these compounding approximations and inaccuracies is that information about electron temperature via the absolute intensity in the center of an optically thick resonance line rarely leads to correct values. This is the case in spite of the preferred exponential temperature dependence in equation 16. Plasma electron temperatures are most frequently arrived at through

continuum diagnostics which tend to be more reliable. Further discussion of line radiation will be confined to its relation to plasma impurities.

The shape and intensity of the x-ray continuum spectrum due to transitions within a given ionic state are determined by the interaction of the following transitions:

(1) **FREE-FREE TRANSITIONS** are the result of acceleration of electrons due to scattering by the Coulomb fields of other charged particles (usually ions). Since the initial and final states of the electron are continuous, the subsequent **Bremsstrahlung** (braking radiation) is also continuous. Intensity is dependent on the square of the nuclear charge (Z^2).

(2) **BOUND-FREE TRANSITIONS** are produced by radiative capture of an electron and the subsequent emission of a photon. These transitions also give rise to a continuous spectrum but with absorption/emission edges at wavelengths corresponding to the appropriate ionization potentials. This radiation spectrum has essentially the same shape as the Bremsstrahlung spectrum, but the **recombination** spectrum dominates at short wavelengths due to its intensity dependence on the fourth power of nuclear charge (Z^4).

(3) **BOUND-BOUND TRANSITIONS** characterize electron jumps between energy levels of the same ionic state. The discrete nature of initial and final states results in **line radiation.** The intensity of this radiation is dependent on the sixth power of nuclear charge (Z^6) and consequently, it predominates at the frequencies at which it occurs.

These radiative transitions are illustrated in Figure

5 for the radiation spectrum of a hydrogen plasma contaminated by 2% oxygen. If impurities are present in the target material (e.g. high Z elements like oxygen), recombination and line radiation obscure the free-free radiation, particularly near the short wavelengths where excitation energies of the higher Z ions are of the order of kT_e. Equation 16 shows that as E_{n^1} approaches kT_e from the high side, I_L becomes increasingly large. For a 1keV plasma containing only 1% oxygen ions with one remaining electron (O_{VIII}, Z=8) line radiation is approximately 300 times the minimum Bremsstrahlung radiation. If steady-state ionization were reached by completely stripping the Oxygen ions, the Bremsstrahlung radiation would increase only by a factor of 3 at 1.5keV. Aside from small effects due to the Gaunt factor, recombination radiation has the same spectral shape as Bremsstrahlung, except for low frequency cutoffs when the energy of the emitted quantum equals an ionization energy of the emitting ion. The reaction rate for each of the two transitions is a function of temperature and density but the role of each process varies considerably for different temperatures and different spectral regions. As a result of the complicated nature of electron temperature/radiation intensity dependence, radiation intensity over certain spectral ranges can be only a weak function of temperature. However, the absolute intensity of those same spectral ranges can be used to determine density even if minimal temperature information is available. Plasma density is most readily measured in the visible spectral range where the temperature dependence reduces to $T_e^{-1/2}$. The strong exponential dependence of the spectrum in the neighborhood of the short wavelength cutoff implies that the most sensitive temperature measurements can be made in the x-ray

region[5].

Bremsstrahlung and recombination transitions with Maxwellian velocity distributions exhibit emission coefficients which are functions of plasma density, nuclear charge, electron temperature and the Gaunt factor for each respective transition. The Bremsstrahlung spectrum increases without limit in the long wavelength direction. The Maxwellian assumption can be made because in the process of electrons radiating, the time between emissions is usually longer than the time between collisions with other electrons. The high collision rate presumes a near Maxwellian distribution function. Emission coefficient for Bremsstrahlung radiation (per unit frequency interval per unit volume of plasma in a solid angle 4π) is

$$I_{ff}(\nu) = AZ^2 n_i n_e g_{ff} (E_H/kT_e)^{1/2} \exp\{-h\nu/kT_e\} \qquad (17)$$

where g_{ff} is the Gaunt factor for the free-free transitions, A is a numerical factor equal to 1.7×10^{-40} erg cm^3, n_i and n_e are ion and electron densities and E_H is ionization energy of Hydrogen (13.58eV). The Gaunt factor represents the departure of the quantum-mechanical calculation from the classical result and is averaged over the Maxwellian velocity distribution at the electron temperature T_e. It varies between 1.39 and 1.16 for T_e between 100eV and 5keV and approaches 1.103 at higher temperatures. As a first approximation, g_{ff} is usually set equal to 1.

Converting equation 17 to emission per unit wavelength interval yields

$$I_{ff}(\lambda) = 1.9 \times 10^{-28} Z^2 n_i n_e g_{ff} \lambda^{-2} (kT_e)^{-1/2} \exp(-hc/\lambda kT_e) \quad (18)$$

Total radiated Bremsstrahlung power is obtained by integrating this over all wavelengths,

$$P_{ff} = 1.5 \times 10^{-38} (kT_e)^{1/2} g_{ff} n_e n_i Z^2 \quad (19)$$

where T_e is in electron volts.

The coefficient for free-free radiation is proportional to continuum intensity which produces a maximum at

$$\lambda = hc/kT_e \quad (20)$$

For long wavelengths ($\lambda >> hc/kT_e$) in the visible range, the spectral shape loses its strong exponential dependence on T_e but retains its $T_e^{-1/2}$ relation. However, for short wavelengths ($\lambda \leq hc/kT_e$ or $h\nu \geq kT_e$), the spectral shape is strongly temperature dependent through the dominant exponential term. When $h\nu >> kT_e$, the logarithm of the spectral distributuion of a continuous spectrum is essentially a staight line whose slope is given by electron temperature kT_e (traditionally plasma temperatures are

quoted in electron volts). This method of determining T_e is widely used in experiments where x-radiation is due to Bremsstrahlung of thermal electrons. A complicating feature, however, is the need for having reliable information on which part of the electron density is responsible for the temperature. If the distribution of particles is rather complicated, the electron temperature, as determined from the shape of the continuous spectrum, may only apply to a small fraction of the plasma being studied.

Frequency dependence of the recombination emission from electron capture into completely stripped ions is approximately comparable to free-free emission in the classical limit. The comparison is made after disregarding quantum mechanical corrections to the classical model and discontinuities in the emission spectrum at frequencies corresponding to the ionization potential of the final state. The emission coefficient of the radiation due to recombination for a level with a principle quantum number K per unit volume of plasma in a solid angle 4π per unit frequency interval is

$$I_{fb}(\nu) = \beta n_i n_e (E_H/kT_e)^{3/2} g_{fb} (E_{iK}/E_H)^2 K^{-1} N$$

$$X \exp\{(E_{iK} - h\nu)\} \qquad (21)$$

where E_{iK} is the ionization potential of the target element or impurity. If the K shell is simple, then the number of empty sites, N, is equal to $2K^2$. Expressing E_{iK} in terms of K and z by the relation

$$E_{iK} = (-13.58Z^2)/K^2 \qquad (22)$$

allows equation 21 to be reduced to

$$I_{fb}(\nu) = \beta Z^4 n_i n_e g_{fb} K^{-3} (E_H/kT_e)^{3/2}$$

$$X \exp\{(E_{iK} - h\nu)/kT_e\} \qquad (23)$$

The fourth power of nuclear charge indicates that free-bound radiation dominates at short wavelengths for plasmas whose components have ionization potentials near kT_e.

For a composite spectrum comprising only Bremsstrahlung and recombination continua, spectral intensities are strongly temperature dependent. If the spectral region is far enough into the short wavelength region where recombination series limits are not a hindrance and if there are negligible impurities, then accurate temperatures can be estimated from x-ray intensities emitted from a plasma. This region is below 14.2Å for the example in Figure 1. At longer wavelengths approaching the visible region, it is clear from equation 17 that as λ increases, ν decreases causing $(-h\nu/kT_e)$ to become small. Hence the exponential approaches 1 and the emission coefficient becomes

$$I_{ff}(\nu) = \beta Z^2 n_i n_e g_{ff} (E_H/kT_e)^{1/2} \qquad (24)$$

but shows no spectral dependence on T_e [29]. Thus in the visible region, electron density can be extracted from the

absolute intensity of emission if $n_i Z^2$ can be determined.

The mechanism for deconvolution of electron temperatures from emission intensities shall be the topic of the next section.

C. PLASMA TEMPERATURE FROM CONTINUUM INTENSITY

The most popular and least complicated method of determining reasonably accurate plasma temperatures is to measure the relative transmission through absorption filters of two or more thicknesses. Since absolute intensities of continuous radiation depend directly on electron densities (equation 28), temperature, which appears in the exponential, can best be obtained from relative measurements of the continuous radiation at different wavelengths.

If equation 18 is reduced to the form

$$I(\lambda) = I_0(\lambda) \exp\{-E/kT_e\} \qquad (25)$$

where E is the x-ray photon energy, it can be seen from the exponential that for electron temperatures in the area of 100eV there is a rather rapid intensity decrease for x-rays in the 1keV range.

$$I(\lambda) = I_0(\lambda) \exp\{-1000/100\} = 4.5\times10^{-5} I_0(\lambda) \qquad (26)$$

This neat cutoff point which is highly temperature dependent is the basis for extracting sensitive temperature measurements from high-energy continuum wavelength distributions.

The position of the cutoff can be varied artificially by placing an absorption filter in front of the x-ray continuum detector. Among all the characteristics of x-radiation, the best known experimentally are the mass absorption coefficients as a function of wavelength and absorber material, shown in Figure 1 for several materials. Materials used in the soft x-ray range are usually Be, Al,

Ni and C because of their relatively high transmission and freedom from an abundance of absorption edges at the desired wavelengths. Filters determine the electron temperature from the slope of the x-ray continuum, when no lines are present in the wavelength region and when an exponential decay of the continuum is expected. Figure 6 shows the K-edge cutoff for 5 and 15 micron Al lies at 8Å and transmits mainly soft radiation whereas a thicker Be foil would transmit harder radiation because of its lack of a K absorption edge. Cutoff energy for an absorber can be determined from the relation[18]

$$\kappa_\nu d = 1 \tag{27}$$

where d is the absorber thickness and κ_ν is the frequency dependent absorption coefficient defined by

$$\kappa_\nu = 2\times10^{-14} Z^4 E^{-3} g_{f^1} n_{i^1} \tag{28}$$

κ_ν has units of inverse centimeters when E is in electron volts. The cutoff energy, E_c, is the energy at which transmission is reduced by a factor of e^{-1}.

The Bremsstrahlung spectrum for a specific temperature which penetrates a foil of thickness d is a product of the emission function (equation 18) and the exponentially dependent transmission function. This product can be written as

$$I(\lambda) = 1.9 \times 10^{-28} Z^2 n_i n_e g_{ff} \lambda^{-2} (kT_e)^{-1/2}$$

$$\times \exp\{(-E/kT_e) - \sum_j \kappa_j d_j\} \qquad (29)$$

where E is the photon energy (hc/λ). Summation of various absorber materials and thicknesses is permitted. Equation 29 has been solved numerically by computer for a range of foil thicknesses, various foil materials, and several electron temperatures[5-7]. A typical set of curves for Aluminum plotted by Elton using the NRL NAREC computer is shown as Figures 2 through 23 of reference 7. Foil thicknesses in equation 29 are in mg/cm^2. These can be converted to inches using the graphical conversion of Figure 7.

The curves of relative Bremsstrahlung emission versus wavelength are extremely useful in choosing foils for viewing specific spectral regions and for masking off line radiation from impurities. Minute amounts of Oxygen (O_V and O_{VI}) for example will produce copious amounts of radiation in the 150 to 170Å region. Ni foil which is essentially opaque at 150Å will serve to determine if these impurity elements are a problem.

If the integration of the transmission function in equation 29 is performed over photon energy, E, a plot could be made of Bremsstrahlung transmission (normalized to d=0) versus foil thickness for various electron temperatures. The energy flux received by the detector is essentially

$$F(d) = \theta \int_0^\infty \exp\{-(E/kT_E) - \kappa d\}\, dE \qquad (30)$$

where θ acccunts for all the factors left out in the transitior frcm equation 29. Between absorption edges, κ varies as E^{-3} frcm equation 28. Rewriting equation 30 as

$$F(y) = \theta \int_0^\infty S(E) \exp\{-\kappa(E)\, y\}\, dE \qquad (31)$$

where $S(E)$ is the spectral distribution function I_{ff} minus scme constants which are lumped into θ, and substituting in fcr $\kappa(E)$ resclts in the energy detected behind thickness y

$$F(y) = \gamma \int_0^\infty S(E) \exp\{-E^{-3} y\}\, dE \qquad (32)$$

γ is a cconsclidation of constants from equation 28 with thcse in θ. Ihe thickness y has been substituted for d for ease of nctaticn in fcrmulae. Differentiating both sides with respect tc y yields

$$dF(y)/dy = -\gamma \int_0^\infty S(E)/y\{E^{-3} y \exp(-E^{-3} y)\}\, dE \qquad (33)$$

For each fcil thickness y there is a cutcff energy E_y determined by equaticn 27 at which the term

$$E^{-3} y \exp(-E^{-3} y)$$

has a sharp maximum. Therefore at that energy, equaticn 33 can be approximated by

$$dF(y)/dy = -\xi y^{-1} S(E_y) \qquad (34)$$

This equation written in the form

$$S(E_y) = -\xi^{-1} \{dF(y)/dy\}_y \qquad (35)$$

provides a transition from a plot of $S(E_y)$ versus λ for a specific temperature and thickness, to a plot of F(y) (which has been integrated over photon energy) versus foil thickness y , as illustrated in Figures 24 through 39 of reference 7. Graphs of F(y) versus y can be used to obtain values for ratios of intensities transmitted through two different foil thicknesses at different temperatures, resulting in a plot of two foil transmission ratio versus electron temperature. Experimentally obtained transmission ratios can be applied to this curve to pick off a plasma electron temperature from the abscissa.

Transmission curves for the Brensstrahlung spectrum may be combined to yield the transmission through multiple foil layers. However, integrated relative intensities versus foil thickness cannot be easily combined and curves must be plotted for each specific ratio.

A superficial acquaintance with x-ray measuring techniques often leads to the erroneous conclusion that it is a straightforward matter to interpret data obtained by simple measurements. A unique analysis, however, can only be carried out if sufficiently precise data is available on the shape of the spectrum and the radiation energy, in absolute units. Determination of electron temperature through the mean energy of photons passing through filters leaves a wide margin for error if recombination radiation due to impurities is not considered. A small amount of Oxygen (usually the most prevalent impurity), some of which

may be fully ionized, can produce recombination radiation which exceeds the bremsstrahlung radiation in the energy range 900 to 1000eV by several orders of magnitude. Measurements with filters of Al and Be would yield a temperature of the order of 1keV whereas the actual temperature is only several tens of electron volts. This obviously is cause for extreme caution to be exercised in preparation of experiments and analysis of data to ensure elimination of miscalculation.

IV. EXPERIMENTAL PHASE

A. LASER SYSTEM

The laser used to produce plasmas in this temperature investigation was a Korad K-1500 Neodymium-doped glass Q-switched laser system. The basic components of the K-1500 system were the Korad K-1Q Q-spoiled laser retrofitted for Nd-glass lasing rod application, the K-QS2 Pockels Cell assembly with associated shutter electronics used for Q-switching, and the Korad K-2 laser head with flash-lamp firing electronics and fire signal delay circuit. Expansion optics were required to expand and collimate the K-1Q oscillator pulse from the 0.5 inch diameter oscillator rod so that it would couple with the 0.75 inch diameter rod of the K-2 amplifier. The fire signal delay circuit synchronized the arrival time of the K-1Q pulse at the K-2 head as maximum population inversion was attained in the K-2 lasing material. A complete description of the laser system is available in reference 30.

Energy output of the system for various phases of the experiment ranged from 3 to 13.5J. Pulse duration was consistently 25nsec (FWHM) giving an output power level range of 120 to 540MW. Shot to shot energy variation at all levels within the operating range was approximately 10% of the nominal setting.

B. LASER MONITORING TECHNIQUES

The laser pulse was monitored with a Korad K-D1 rapid response planar diode which provided a signal proportional to the laser power. It also integrated this signal to provide an output which was proportional to the laser energy. About 1% of the laser output beam was reflected by a

quartz beam splitter to a MgO diffusing block for viewing by the K-D1 as a point source whose intensity attenuated as R^{-2}. Scattered light from the diffuser was passed through a 0.1% neutral density filter before entering the photodiode.

The power signal from the photodiode was displayed on a Tektronix 7904 oscilloscope. This signal was used to determine the full width at half maximum amplitude (FWHM) duration of the laser pulse. Peak output power was determined by dividing laser energy by the FWHM duration. No variation in FWHM duration of the power signal was observed during the period of experimentation.

Energy output of the laser, at a point immediately after the pulse had passed through the beam splitter, was displayed on a Tektronix 564B storage oscilloscope. The photodiode energy signal was calibrated by McKee[25] using a Westinghouse RN-1 Laser Radiometer placed to interrupt the laser pulse passing through the beam splitter. The radiometer provided an absolute measure of the energy of the laser pulse beyond the beam splitter which allowed calibration of the voltage reading on the storage oscilloscope. Energy output was monitored on every shot because of its poor reproducibility.

Energy loss through the focusing lens at the vacuum chamber was estimated from a transmission curve to be 5%. The loss through the chamber window was measured using a Beckman spectrophotometer and found to be 20% for a wavelength of 1.06 microns. These losses necessitated reducing the energy reading on the storage oscilloscope by a further 24%. The energy range mentioned in section A was reduced to an experimental variation of about 90 to 410MW.

C. INTERACTION CHAMBER AND TARGET

The laser pulse was focused by a Hoya, coated camera lens, effective diameter 49mm and power of +3 diopters, through a 3mm quartz vacuum chamber window on to the surface of a solid target. The vacuum chamber was originally constructed by McKee[25] to facilitate the use of magnetic probes. The inside volume of the chamber was cylindrical with a diameter of 25cm and a height of 15cm. Chamber dimensions and target positioning are shown in Figure 8. All ports are circular.

For all temperature measurements, the chamber was evacuated to approximately 2×10^{-5} Torr of air by an oil diffusion pump, the description and operation of which are detailed in reference 31. The portion of this experiment requiring an ambient background pressure were conducted by first evacuating the chamber to 10^{-6} Torr and then introducing Nitrogen gas through a needle valve to pressures varying from 20 to 4000 microns.

The laser beam was focused to a spot size of 127±17 microns radius at top dead center of the circular front surface of the target. Path of incidence was 30 degrees from normal. The original intent of the incident angle was to permit close orientation of magnetic probes with the targets surface while avoiding interaction with the laser pulse. The angle also eliminates feed back into the laser system due to reflection from the target's surface which prevents relaxation oscillations being set up between the target and other reflecting surfaces in the amplifier chain. Focusing was achieved by simulating the Nd laser beam with a Helium-Neon laser and observing the spot on the plane

surface of the target. Because of the longer wavelength of the Nd laser the separation between the focal planes of the Nd and He-Ne wavelengths was approximately 0.5mm[27]. This change was compensated for by focusing the He-Ne beam on the target surface and then advancing the lens by 0.5mm. This method is accurate to ±1mm.

The target for all phases of experimentation was a flat, polished disc of Aluminum 6mm thick and 6cm in diameter. The target surface was prepared under vacuum immediately prior to taking data by illuminating it with laser pulses which were focused by a +2 diopter lens. The target was rotated after each preparation shot. This form of cleaning was intended to remove contaminants and oxides from the Aluminum surface.

D. DIAGNOSTIC APPARATUS

X-ray emission from the laser generated plasma was detected by two semiconductor diodes in probe mountings placed symmetrically in a horizontal plane with their axes at 7 degrees from the normal to the target surface (see Figure 9). The acceptance angles of the detector windows were defined by circular apertures of diameter 0.8cm located 17cm from the focal region of the target.

1. Probe Assembly

An exploded view of a single probe assembly is shown in Figure 10. It consists of an aperture, light seal gaskets and filter retaining ring, a filter holder body, a light shield, a detector, and a N-type to BNC adapter. The aperture was fastened to the filter holder body with four machine screws. The K-edge filter was sandwiched between a neoprene gasket in the aperture and a filter retaining ring

which pressed tightly against the filter holder. A second larger neoprene gasket around the periphery of the aperture further ensured light-tight contact of the filter against the filter holder. The filter holder had six holes drilled radially on its circumference to provide for vacuum pumpout. The two piece light shield provided baffling to prevent light from entering the detector through the pumpout holes. Interior surfaces were finished in matte black enamel. The front half of the light shield screwed onto the filter body and the assembly in turn screwed into the detector assembly which consisted of a PIN diode and BNC adapter. The rear half of the light shield slipped over the rear of the assembled portion and formed a press fit, O-ring connection with the front light shield. The filter was positioned away from the detector to reduce fluorescence radiation effects from high Z filter materials.

The two probe assemblies were press fit fastened to two vacuum bulkhead BNC connectors mounted at angles of 7 degrees from normal to a 1.3cm thick Aluminum plate (see Figure 11). The plate was designed to be mounted in chamber window #5 directly opposite the target surface. Electrical connection to the probes was made through the vacuum bulkhead BNC connectors.

2. PIN Diode Detectors

Detectors used in these experiments were 050-PIN-75 double Diffused Silicon Photodiodes[32] with a depletion depth of 75 microns, a dead layer equivalent to 0.4±0.2 microns of silicon, and an entrance window of 50mm^2.

The PIN photodiode is the most common depletion-layer photodetector because the depletion region thickness (the intrinsic layer) can be tailored to optimize the sensitivity

range, the frequency response, and the efficiency (see Figure 12). This type of diode is made by lowering the doping in the epitaxial layer of the abrupt-junction diode. It is well suited for use with pulsed plasma devices because of its inherently fast rise time and high detection sensitivity. The rise time is related to the square of the depletion depth divided by the bias voltage and is approximately 1.5nsec for a 75V bias[33]. Because the hole collection time is longer than the electron collection time, the decay time is approximately 3nsec. Combined rise time of the diode, cables, and oscilloscope was approximately 2nsec.

Figure 13 shows the energy levels of a reverse biased PIN diode and a schematic for a single channel of the detector system. Absorption of x-ray photons in the intrinsic region liberate electron-hole pairs which travel in opposite directions and result in a charge output proportional to absorbed photon energy. The detector was biased at -75V through a 10K ohm resistor. Negative biasing produces a positive output signal.

3. K-Edge Absorption Filters

Thin foil discs of Aluminum and Beryllium, 1.3 cm in diameter, were used as filters for the absorption measurements. Aluminum discs were cut from sheets of common wrapping foil available in a variety of thicknesses depending on the commercial brand. Single layers of these foils ranged from 1.83 to 8.54mg/cm^2 in thickness. The thinnest foil, not available commercially, was obtained from the LINAC Laboratory at NPS. The Beryllium foil was obtained from two sources. A 5cm Be disc was cut, using a diamond glass bore, into eight 1cm diameter discs which were then

chemically etched by the method outlined in Appendix A to thicknesses ranging from 8.9 to 46.6mg/cm^2. A set of commercially rolled Be foils 1.45mg/cm^2 thick was purchased from KBI[34].

The foil thicknesses were determined by weighing a measured area of the material on a semi-micro analytical balance and were accurate to 5%. All foils were visually examined in a darkroom with a point source light to ensure freedom from pinholes. Foils were discarded after ten shots to prevent a buildup of debris from altering the effective area of the entrance window. This procedure limited the number of temperature readings which could be obtained with the more scarce and much more expensive Beryllium foil. Table I lists some of the foils used, their thicknesses, and their approximate cutoff energies.

TABLE I

Material	Thickness (mg/sqcm)	Cutoff Wavelength (Angstroms)	Cutoff Energy (eV)
Be	5.80	21.0	600
Be	23.90	13.0	900
Be	66.89	8.7	1450
Al	1.83	25.5	500
Al	8.80	13.5	950
Al	17.08	11.0	1150

(cutoff values for kT=250eV)

4. Probe Monitoring

Signals from both probes were displayed simultaneously

on a Tektronix 7904 oscilloscope by delaying the signal from probe #2 by 80nsec using a combination delay box and delay cable. Figure 14 shows the wiring of the probes from the chamber to the oscilloscope. RG58A cable was used throughout. The signal from probe #1 was relayed through its bias network to the (+) input of a differential comparator in the oscilloscope. Probe #2 signal was passed through a 36nsec delay cable, into a delay box set at 44nsec, through its bias network, into an inverting transformer, and into the (-) input of the differential comparator. Both signals entered the oscilloscope through 50 ohm termination resistances. The oscilloscope was triggered by a signal from the K-D1 photodiode being passed through a 332cm cable to the oscilloscope time base input.

All temperature data were taken with a horizontal time scale of 20nsec per division which allowed for estimates to within 2nsec. Vertical voltage scale adjustments were varied between the maximum attainable gain of 5V per division and 20mV per division. The lower limit was determined by the noise level at which the signal was no longer discernible from background interference. Shielding of signal leads did not reduce the noise level.

Attenuation of the probe signal was attempted using both an ordinary 2W carbon resistor and a variable high frequency attenuator. In each case the distortion of the pulse was severe. This development coupled with the noise problem at high gain placed a limit on the thickest and thinnest foils which could be used for temperature measurements. The limits for Aluminum were 1.83 to 17.08mg/cm^2 and for Beryllium were 5.80 to 66.89mg/cm^2.

Delays of the various signals to the oscilloscope are given in Table II. The values were calculated based on the

assumption that the speed of the signal in the cable is two thirds that of light in air, that the delay through a diode is 1nsec, and that there is negligible delay at the target.

TABLE II

Delay Phase	Probe #1	Trigger
splitter to diode	68cm/2.3nsec	120cm/4nsec
delay in diode	(PIN) 1nsec	(K-D1) 1nsec
delay to scope	341cm/17.1nsec	332cm/16.6nsec
TOTAL DELAY	20.4nsec	20.7nsec

The delay times (excluding delay through the diodes) were verified to within 1nsec using a pulse reflection technique on a Tektronix 519 oscilloscope. Within the accuracy of time base readings the signal from probe #1 at the oscilloscope was assumed to coincide with triggering of the horizontal sweep.

5. Vacuum Photodiode

An x-ray vacuum photodiode (VPD), theoretically capable of less than 1nsec time resolution, was constructed following the basic design outlined in reference 16. Original intent of construction was to produce a detector capable of supplementing the expensive PIN diodes. The finished VPD, however, proved to be too cumbersome to be used in conjunction with existing detector arrangements. This was primarily the result of continuous modifications made necessary by lack of suitable materials and micro manufacturing techniques.

Figure 15 shows the basic construction of the diode and electrical connections. The photocathode C was the

gold-coated inner surface of a 6cm long 1cm diameter brass cylinder. Gold was chosen for stability and high photoelectric efficiency. With a plasma located on the cylinder axis 10cm from the cathode midpoint, radiation struck the cathode at angles of incidence between 87.8 and 85.9 degrees from normal. The anode A was a 0.6cm diameter brass cylinder which was capacitively coupled to ground through a 0.05cm thick Teflon sheath around a 0.4cm diameter grounded brass rod G. The sheath and cylinder were swaged into place around the ground potential rod. The structure was surrounded by a cylindrical stainless steel screen S_1 also at ground potential. A second independent ground screen S_2 surrounded the diode and its cables, and an outer screen S_3 acted as a housing and was at the potential of the vacuum chamber. The three screens were separated by cylindrical layers of nylon insulation. The screen S_3 isolated the diode from electrostatic disturbances due to the laser plasma since it was sealed off by the metal foil F. The aperture and foil retaining mechanism were identical to that described in subsection 1. The signal was fed to a RG174 coaxial cable SIG with the ground screen common to S_1 and G. 2KV high voltage was applied to the anode through a RG62 coaxial cable HV.

Signals were monitored in a manner similar to that described in subsection 4. Cables were adjusted so that arrival of the diode signal coincided with triggering of the oscilloscope. Considerable noise was encountered at vertical gains of more than 500mV/cm. Screening of the signal cable did not suppress the noise component.

Figure 16 shows the VPD pulse in relation to the laser pulse. The pulse compares favorably with that in reference

16 in its relation to the laser pulse. The shape is seen to follow the shape of laser pulse as in reference 16 if the noise component is ignored. Temperature data was not taken with the VPD because of its incapatibility with the smaller PIN diodes.

E. EXPERIMENTS PERFORMED

1. Plasma Temperature Measurements

The primary purpose of this study was to determine the temperature of an electron laser produced Aluminum plasma and to ascertain whether a suprathermal component existed within the plasma. Data required for temperature measurements was obtained by photographing probe signals displayed on the Tektronix 7904 oscilloscope and submitting the photographs to analytical measurements. A typical pair of x-ray pulses and the corresponding laser power pulse are shown in Figure 17.

Ratio measurements of the peak amplitudes of the probe signals were required for temperature evaluation. The procedure was to first use equal values of equivalent Aluminum absorbing mass in both channels. Thirty-five signals V_1 and V_2 were recorded and the signal ratios V_1/V_2 measured and averaged to give a mean value R and a root mean square deviation $\pm\Delta R$. This gave a temperature independent normalizing constant. To measure a temperature sensitive ratio the absorber mass screening one channel was changed to a suitable value and signals V_1' and V_2' were recorded. The required transmission ratio was then RV_1'/V_2'. For each pair of foils, ten ratios were recorded and averaged.

A computer program was written to plot curves of theoretical transmission ratios for a particular pair of foils versus electron temperature. The program was given data extracted from reference 7 which was then applied to a Least Squares polynomial evaluation to provide an eleventh degree polynomial fit of the data points. The experimentally obtained transmission ratio was read in and applied to the ordinate and the polynomial was evaluated on an iterative basis until a corresponding ratio and accompanying temperature were located. This process was repeated for 8 Aluminum and 5 Beryllium foil pairs (see Figures 18-30).

The computer program also plotted isothermal curves of relative Bremsstrahlung transmission versus foil thickness for both Al and Be. The relative transmission was normalized to transmission through the thinnest Al and Be foil rather than to transmission through zero foil thickness. These curves were used to determine whether or not any suprathermal activity was present in the plasma (see Figures 31-32). The computer program is outlined in Appendix B.

Frequent null checks were made by placing a thick glass plate in front of each probe. The plate would attenuate an x-ray signal but would permit detection of light leaks in the probe. The normalizing ratio R was measured after every third foil pair. Its dependence was primarily on the geometrical relation between the two probes and the plasma plume.

The photographs taken for temperature measurement were also used to determine the shape, the start time and the FWHM of the x-ray pulse, and they provided data for a plot of temperature versus laser flux density shown in Figure 33.

2. Time Resolved Temperature

A series of photographs was taken with the horizontal time base expanded to 10ns in order to obtain pulse ratios which could be related to time. Foils in probes #1 and #2 were 6.97 and 8.54mg/cm^2 Al respectively. The time resolved temperature is plotted in relation to the time resolved laser power pulse in Figure 34.

3. Pressure Dependence

The dependence of x-ray intensity on the ambient background pressure was determined by taking five shots at each of 14 pressures ranging from 20 to 4000 microns of Nitrogen gas. The x-ray intensity of each shot was divided by the energy for normalization and the five normalized intensities were averaged. Aluminum foil of density 6.97mg/cm^2 was used as a filter. Figure 35 shows a plot of x-ray intensity in arbitrary units per joule versus ambient background pressure.

4. Temperature/Magnetic Field Correlation

Simultaneous temperature and spontaneous magnetic field measurements were taken while focusing the laser at the same spot for 25 successive shots. The two probes were mounted vertically to obtain the same view of the cavity which was being bored along the axis of the laser beam (30 degrees from normal). The adhoc probe arrangement placed them at an angle of 17 degrees from normal (or 13 degrees off the laser axis) providing the best possible view of the cavity as it was being created (see Figure 36). A magnetic probe was in

place against the target directly above the focal spot. Its position did not obscure the path of x-rays to the probes. A complete description of equipment layout and data correlation for this combined experiment is provided by Williamson[35].

V. RESULTS AND CONCLUSIONS

An experimental study was made of the plasma temperature and related phenomena of a laser produced Aluminum plasma. Electron temperatures derived from the x-ray flux ratios measured by two detectors with various combinations of Aluminum-Aluminum and Beryllium-Beryllium absorption foils are listed in Table III.

TABLE III

Foil	Thicknesses (mg/sqcm)	Energy (J)	Temperature (eV)
Al	1.83/3.66	9.9(13.0)	148
Al	3.66/5.50	9.9(13.0)	148
Al	3.66/4.30	9.7(12.8)	136
Al	6.97/8.54	10.0(13.1)	172
Al	8.80/10.37	9.7(12.8)	148
Al	10.37/13.94	10.0(13.1)	181
Al	13.94/17.08	9.3(12.2)	185
Al	12.91/15.77	9.5(12.5)	178
Be	5.80/8.96	9.8(12.9)	144
Be	8.96/13.59	9.7(12.7)	162
Be	15.30/23.90	10.0(13.2)	159
Be	34.02/46.62	10.2(13.4)	180
Be	46.62/66.89	9.0(11.8)	162

(the energy value in() is prior to the 24% reduction discussed in section IV. B)

It was found that the temperatures inferred from the various metal foil combinations were generally the same to within ±10%. Evaluation of the thirteen different temperatures in Table III averages to 162±17eV as the best fit of the experimental absorption data to the transmissions

expected for Aluminum Bremsstrahlung. The contours of experimental data points in Figures 31 and 32 follow very closely those of the theoretical continuum data, indicating that the plasmas observed had equilibrium electron distributions. A tendency of experimental points to cross the theoretical curves towards increasing temperature as foil thickness increased would have been an indication of a non-Maxwellian distribution within the plasma. This occurs because ratios of absorber foil detectors indicate higher temperatures for foils with higher cutoff energies when a Maxwellian distribution is assumed. For the plasmas observed it can thus be assumed that the x-ray spectral distribution was nearly that of a Bremsstrahlung continuum in the wavelength interval 5 to 30Å with no significant line contribution.

Results of temperature measurements confirm that temperatures determined by the two foil method are not independent of the foils used. A wider separation in cutoff energies of the two foils produced higher electron temperatures as is seen from the Al foil pairs (3.66/5.50) and (3.66/4.30) in Table III. The foil pairs used throughout the experiment, however, were considered to be sufficiently close in cutoff separation that averaging of temperatures obtained from the various pairs was permissible. For cutoff separations of more than a few Angstroms the temperatures would have to be considered unique and reported as individual temperatures for different electron groups within the plasma.

Errors accumulated in ratio measurements were typically 5% in reading the oscilloscope photographs, 4% from the relative sensitivity normalization of the two detectors, 7% in plotting transmission ratio curves, and 4% in measuring the thickness of the absorption foils. The net error in the ratio is then 19% giving a temperature to approximately ±10%

accuracy.

The x-ray pulse commenced at a point 24nsec after the laser beam illuminated the target when the plasma became optically thick (see Figure 17). The pulse had a FWHM of 18nsec with a rise time of 10nsec. The peak of the x-ray pulse and the peak of the laser power pulse both occurred at 50nsec after formation of the plasma. A time resolved temperature study showed that the peak temperature occurred approximately 4nsec after the peak of the laser pulse or 54nsec after formation of the plasma.

Temperature values deduced from the ratio measurements were used to plot the variation in electron temperature with laser flux density (see Figure 33). On the basis of these data the exponent of the power law relating temperature to flux density was calculated to be 0.404. This value is below the theoretical 4/9 steady state scaling relation to an extent which is not quite compatable with estimated temperature errors. The origin of the discrepency is believed to be a resultant of two basic factors. The first is the limited range of laser energy for which temperatures could be recorded. This limitation would not allow for establishment of a definite trend in the temperature/flux relationship, hence the data sample could perhaps be considered too small to define a power law.

A second, more subtle factor is that the x-ray intensities being measured are effectively time and space integrated by the detection system. The emission zone will be spatially and temporally smaller for the harder x-rays which are associated with regions of high temperature. Because of the different transmission characteristics of the two absorber foils the effective emission zone as seen by the two diodes will have different volumes. The smaller effective zone corresponds to the foil which transmits

predominantly harder x-rays. However, the detector signal ratios are interpreted and adjusted on the assumption that an equal emission volume is seen by each detector. The difference in emission volumes leads to an over estimate of the ratio of emission coefficients and hence an under estimate of temperature. The result would be a downward shift in the slope of the temperature/flux density graph.

Preliminary background pressure measurements showed an increase in x-ray intensity with increasing pressure from 10 microns up to about 300 microns with intensity per joule in arbitrary units being related to pressure by a scaling factor of 1/4. Beyond 300 microns the intensity dropped off sharply (see Figure 35). The increase in observed x-ray intensity corresponds to a similar increase in the magnetic field intensity over the same pressure range[26], where the scaling between magnetic field and ambient plasma density is about 1/3. The striking similarity between the two seemingly independent experiments is not fully understood, although it is noted that absolute x-ray intensity can be related to plasma density. The intensity measurements here cannot be given absolute values.

X-ray intensity readings taken while a crater was being bored into the target indicated that the temperature remained constant over the 25 shot range of the experiment. From the combined temperature/magnetic field measurements taken as the crater developed, Williamson was able to calculate a magnetic field strength which compared to within 20% with the field that was simultaneously measured (see reference 35).

The overall view of data gathered through x-ray analysis would indicate that the plasmas observed were very ordinary, low temperature plasmas of the type to be expected

with laser flux densities of 5×10^{11} W/cm^2, since threshold for suprathermal activity is greater than 10^{13} W/cm^2. The electron velocity distributions were Maxwellian with no indications that non thermal components were present.

VI RECOMMENDATIONS FOR FURTHER STUDY

The next obvious step in improving the x-ray diagnostic facility would be the absolute calibration of detectors with an accurately known source. Once this is accomplished, a Ross filter system could be constructed which would provide the type of spectral analysis tool being used in plasma laboratories throughout the world. Absolute intensity measurements would lead directly to very accurate temperature readings, and indirectly to a means of determining plasma densities and detecting suprathermal electron groups.

There is a definite need to establish a capability for determining spatial energy resolution of the plasma. Present emission intensities are not sufficiently strong to permit the use of an ordinary pinhole camera, but with improved focusing of the laser beam on the target this problem could be overcome. There are, of course, various methods of collimation which have proven effective in gathering x-rays for spatial resolution. These would be more costly than a pinhole camera setup but the results would be immediate.

More research of a combined nature would be a definate asset to the NPS Plasma Facility. Simultaneous magnetic field, background pressure, and plasma temperature measurements could provide correlation to data previously accepted without corroboration. The very limited collaboration on magnetic field/temperature measurements proved to be quite useful and contributed to a broadening of each field of research with very little extra effort. More extensive, better planned collaboration would most certainly be of benefit to the students involved and to the school.

The vacuum photodiode constructed as part of this study can be made to work effectively with a little more engineering refinement. It would be extremely beneficial to continue the study of high resolution detectors such as this since they will be a vitally important diagnostic tool as laser pulses continue to narrow.

APPENDIX A

The procedure used to etch the Beryllium foil was based on a Dow Chemical process [36] for chemical milling of Be for removal of machining damage. Techniques and solution quantities were suitably scaled down to meet the limited laboratory quantities required.

Approximately one litre of Dow Chemical Milling Solution A was prepared as follows:

750 (±15) millilitres per litre of phosphoric acid (H_3PO_4) (85%)

71 (±2) grams per litre of chromic acid (CrO_3) (99% chromic trioxide)

200 (±5) millilitres per litre of water (H_2O) (distilled or deionized)

30 (±2) millilitres per litre of sulfuric acid (H_2SO_4) (95 to 98%)

The chromic acid was not added to the solution until immediately prior to etching so that its strength would not be diminished.

Under the cover of a fume chamber, for each etching, 100ml of solution A was poured into a watchglass and the foil to be reduced was immersed in the solution. Floatation was caused by bubble formation on the underside of the foil necessitating frequent inverting of the foil using tweezers.

The solution and resulting fumes were extremely toxic. Gloves, goggles, and a respiratory mask were worn at all

times during the process.

The rate of etching was measured with the aid of a stopwatch and micrometer and determined to be 500 microns per minute at 21°C for each surface of the foil including the edge.

APPENDIX B

The following computer code has been compiled to aid in reduction of x-ray emission data which was obtained during electron temperature measurements. It has been written specifically for measurements using combinations of Aluminum foils. A similar program with minor modification was used to reduce data obtained with Beryllium foils.

The code is divided into two parts. Part A is designed to plot the ratio of Bremsstrahlung radiation transmitted through two Aluminum foils of different thicknesses versus logarithm of electron temperature. Data for this type of plot was obtained from Figures 24, 25, 27, and 28 of reference 7 by selecting a desired foil thickness and picking off the Bremsstrahlung transmitted at temperatures varying from 100eV to 2KeV. Examples of similar computer plots are shown in Figures 28 and 29 of reference 6. Once each curve has been plotted, an experimentally determined transmission ratio for the particular pair of foils being examined is read into the program and a plasma electron temperature is calculated.

Part B of the code produces a plot of normalized Bremsstrahlung transmission versus foil thickness for various temperatures. These curves differ from those of reference 9 in that they are normalized to transmission through the thinnest foil rather than transmission through zero thickness.

Both parts of the code make use of the subroutines LEAST and EVAL to fit data to a polynomial approximation. Subroutine LEAST and the function EVAL calculate the least squares polynomial approximation to a set of data specified by the matrix, X, of M nodes with corresponding function

values and weights in the vectors F and W. The weights must all be positive. The polynomial approximation is determined in LEAST and evaluated in EVAL. On input EPS is the desired weighted RMS error. The code increases the degree of fit in an attempt to meet this error request. On return EPS is set to the weighted RMS error of the fit. Because EPS is used for both input and output it must be a variable in the calling program. MAXDEG is the highest degree of fit allowed and must be less than or equal to (M-1). The actual degree of fit is returned in NDEG unless the code is forced to produce a fit MAXDEG by setting EPS negative on input. The vector ARRAY specifies the orthogonal polynomial fit and provides working storage. The dimension of ARRAY in the calling program must be at least (2M+3MAXDEG). The vectors representing X, F, W, ARRAY, and R must be dimensioned in the calling program.

Function EVAL evaluates the orthogonal polynomial fit computed by LEAST and specified by vector ARRAY. The fit of degree N is evaluatd at the arguement Y. N must be less than or equal to NDEG as returned from LEAST. LEAST is called only once for each fit, but EVAL is called once for each argument at which a value of the fit is required. MAXDEG must have the same value as in the call to LEAST.

Description of arguments:

E — the electron temperature of interest, read in as data

W — a weighting factor required by subroutine LEAST (all values set equal to 1)

X — the matrix of transmission values for 14 foils at 10 temperatures, read in as data

TR — the matrix of calculated transmission ratios

ELOG — the natural logarithm of E

RATIO	the vector of transmission ratios calculated by EVAL
ELCGT	the vector of the natural logarithm of temperatures used by EVAL to calculate RATIO
ARRAY	a working vector used by LEAST
TTR	a dummy vector used to hold columns of the matrix TR for calculation by LEAST in part A
TLN	natural logarithm of the normalized transmission through the various foils
DTLN	a dummy vector used to hold columns of TLN for calculation by LEAST in part B
FOIL	a vector of the various foils used (quantities are in milligrams per square centimeter)
FLOG	natural logarithm of foil thickness
THICK	the vector of the natural logarithm of foil thicknesses used by EVAL to calculate RELTR
RELTR	the vector of normalized transmission ratios calculated by EVAL
ETR	the experimental transmission ratios read in as data (one ratio for each pair of foils)
TEMP	the electron temperature calculated from ETR for each pair of foils
M	the number of temperatures used
N	the number of foils used

```
                    *** JOB CONTROL CARDS ***

//ALLM&2&@ JOB (2875,0330,WS44),'S.A. SHEWCHUK',TIME=(00,40)
// EXEC FCRTCLGP,REGION.GO=150K
//FCRT.SYSIN DD *

                    *** MAIN PROGRAM ***

      DIMENSION E(10), W(16),WW(16), X(14,10),
     1 TR(13,10), ELOG(12), RATIO(500), ELOGT(500),
     2 ARRAY(80), TTR(12), TLN(14,10), CTLN(15),
     3 FCIL(14), FLOG(14),THICK(500), RELTR(500),
     4 ETR(14), TEMP(14)

      INTEGER*4 ITB(12)/12*0/
      REAL*4 RTB(28)/28*0.0/
      REAL*8 R(16)/16*1.0/
      REAL*8 TITLE(12)
      EQUIVALENCE (TITLE,RTB(5))
      DATA W/16*1.0/
      DATA TEMP/14*0.0/

  100 FORMAT (10F5.0)
  101 FORMAT (10E8.2)
  102 FORMAT (14F5.2)
  103 FORMAT (6A8)
  104 FORMAT (13F5.2)
  200 FORMAT (10X,F5.0,5X,14F6.2)
  201 FORMAT (14F8.4)
  202 FORMAT (///,10X,'GRAPH',5X,'ELECTRON TEMPERATURE',/)
  203 FORMAT (12X,I1,15X,E12.4)

****** PART A

      M = 10
      N = 14
      READ (5,100) (E(I),I=1,M)
      DO 1 I = 1,N
      READ (5,101) (X(I,J),J=1,M)
    1 CONTINUE
      ITB(3) = 6
      ITB(4) = 8
      ITB(8) = 1
      ITB(10) = 1
      ITB(12) = 1
      N1 = N-1
      DO 3 I = 1,N1
      DO 3 J = 1,M
      IF((I.EQ.2).OR.(I.EQ.4).OR.(I.EQ.6).OR.
     1  (I.EQ.8).OR.(I.EQ.12)) GO TO 2
      TR(I,J) = X(I,J)/X(I+1,J)
      GO TO 3
    2 TR(I,J) = 0.0
    3 CONTINUE
      DO 4 J = 1,M
      WRITE (6,200) E(J), (TR(I,J),I=1,N1)
    4 CONTINUE
      DO 5 J = 1,M
      ELOG(J) = ALOG(E(J))
    5 CONTINUE
      EPS = -1.0
      READ (5,104) (ETR(I),I=1,N1)
      DO 10 I = 1,N1
      IF((I.EQ.2).OR.(I.EQ.4).OR.(I.EQ.6).OR.
     1  (I.EQ.8).OR.(I.EQ.12)) GO TO 10
      READ (5,103) TITLE
      DO 6 J = 1,M
      TTR(J) = TR(I,J)
    6 CONTINUE
```

```
      TTR(11) = 2000.0
      ELCG(11) = 0.0
      TTR(12) = 1.05
      ELCG(12) = 12.0
      NUM1 = M+2
      MAXDEG = 11
      CALL LEAST (NUM1,ELCG,TTR,W,EPS,MAXDEG,NDEG,ARRAY,R)
      ELCGT(1) = 4.70
      KCUNT = 1
      DO 8 J = 1,500
      NUM2 = J
      RATIO(J) = EVAL(ELCGT(J),MAXDEG,ARRAY,MAXDEG)
      IF (KOUNT.EQ.2) GO TO 7
      IF (RATIO(J).LE.ETR(I)) TEMP(I) = EXP(ELCGT(J))
      IF (TEMP(I).GT.0.0) KCUNT = 2
    7 ELCGT(J+1) = ELCGT(J) + 0.01
      IF (ELCGT(J+1).GT.7.00) GO TO 9
    8 CONTINUE
    9 CALL DRAWP (NUM2,ELCGT,RATIO,ITB,RTB)
   10 CONTINUE

****** PART B

      DO 12 J = 1,M
      DO 11 I = 1,N
      TLN(I,J) = ALOG(X(I,J)/X(1,J))
   11 CONTINUE
      WRITE (6,201) (TLN(I,J),I=1,N)
   12 CONTINUE
      READ(5,102) (FOIL(I),I=1,N)
      DO 13 I = 1,N
      FLOG(I)  = ALOG(FOIL(I))
   13 CONTINUE
      READ (5,103) TITLE
      MODCUR = 1
      ITB(1) = 1
      DO 17 J = 1,4
      NUM3 = 1
      DO 14 I = 1,N
      IF((I.EQ.3).OR.(I.EQ.5)) GO TO 14
      DTLN(NUM3) = TLN(I,J)
      FLOG(NUM3) = FLOG(I)
      NUM3 = NUM3 + 1
   14 CONTINUE
      DTLN(NUM3) = 0.0
      FLOG(NUM3) = 0.0
      MDEG2 = 5
      CALL LEAST (NUM3,FLOG,DTLN,W,EPS,MDEG2,NDEG,ARRAY,R)
      THICK(1) = 0.6
      DO 15 I = 1,500
      NUM4 = I
      RELTR(I) = EVAL(THICK(I),MDEG2,ARRAY,MDEG2)
      THICK(I+1) = THICK(I) + 0.01
      IF(THICK(I+1).GT.3.0) GO TO 16
   15 CONTINUE
   16 IF(J.EQ.4) GO TO 18
      CALL DRAWP (NUM4,THICK,RELTR,ITB,RTB)
      MODCUR = 2
      ITB(1) = 2
   17 CONTINUE
   18 MODCUR = 3
      ITB(1) = 3
      CALL DRAWP (NUM4,THICK,RELTR,ITB,RTB)
      WRITE (6,202)
      NUM5 = 1
      DO 19 I = 1,N1
      IF((I.EQ.2).OR.(I.EQ.4).OR.(I.EQ.6).OR.
     1  (I.EQ.8).OR.(I.EQ.12)) GO TO 19
      WRITE (6,203) NUM5, TEMP(I)
      NUM5 = NUM5 + 1
   19 CONTINUE
      STOP
```

```
      END
```

*** SUBROUTINE LEAST ***

```
      SUBROUTINE LEAST(M,X,F,W,EPS,MAXDEG,NDEG,ARRAY,R)
      DIMENSION X(1),F(1),W(1),ARRAY(1)
      DOUBLE PRECISION R(1),SUM,CK,TEMP
      IB=MAXDEG+1
      IBL2=MAXDEG-1
      IC=IB+IBL2
      IOL1=IC+MAXDEG
      I1L1=IOL1+M
      RM=M
      TOL=RM*EPS**2
      NDEG=0
      S=0.0
      SUM=0.0D0
      DO 1 I=1,M
      S=S+W(I)
1     SUM=SUM+DBLE(W(I))*DBLE(F(I))
      RN0=S
      CK=SUM/RN0
      ARRAY(IC)=CK
      ERROR=0.0
      DO 2 I=1,M
      R(I)=CK
2     ERROR=ERROR+W(I)*SNGL(CK-DBLE(F(I)))**2
      IF(NDEG.EQ.MAXDEG)GO TO 14
      IF(EPS.LT.0.0)GO TO 3
      IF(ERROR.LE.TOL)GO TO 14
3     NDEG=1
      ES=ERROR
      SUM=0.0D0
      DO 4 I=1,M
4     SUM=SUM+DBLE(W(I))*DBLE(X(I))
      ARRAY(1)=SUM/RN0
      S=0.0
      SUM=0.0D0
      DO 6 I=1,M
      ARRAY(I1L1+I)=X(I)-ARRAY(1)
      S=S+W(I)*ARRAY(I1L1+I)**2
      TEMP=DBLE(F(I))-R(I)
5     SUM=SUM+DBLE(W(I))*DBLE(ARRAY(I1L1+I))*TEMP
      RN1=S
      CK=SUM/RN1
      ARRAY(IC+1)=CK
      ERROR=0.0
      DO 6 I=1,M
      R(I)=R(I)+CK*DBLE(ARRAY(I1L1+I))
6     ERROR=ERROR+W(I)*SNGL(R(I)-DBLE(F(I)))**2
      IF(ERROR.GT.ES.AND.EPS.GE.0.0)GO TO 12
      IF(NDEG.EQ.MAXDEG)GO TO 14
      IF(ERROR.LE.TOL.AND.EPS.GE.0.0)GO TO 14
      DO 7 I=1,M
7     ARRAY(IOL1+I)=1.0
      NDEG=2
      K=2
8     ES=ERROR
      ARRAY(IBL2+K)=RN1/RN0
      SUM=0.0D0
      DO 9 I=1,M
9     SUM=SUM+DBLE(W(I))*DBLE(X(I))*DBLE(ARRAY(I1L1+I))**2
      ARRAY(K)=SUM/RN1
      S=0.0
      SUM=0.0D0
      DO 10 I=1,M
      ARRAY(IOL1+I)=(X(I)-ARRAY(K))*ARRAY(I1L1+I)
     1  -ARRAY(IBL2+K)*ARRAY(IOL1+I)
      S=S+W(I)*ARRAY(IOL1+I)**2
      TEMP=DBLE(F(I))-R(I)
```

```
10    SUM=SUM+DBLE(W(I))*DBLE(ARRAY(IOL1+I))*TEMP
      RN0=RN1
      RN1=S
      IT=IOL1
      IOL1=I1L1
      I1L1=IT
      CK=SUM/RN1
      ARRAY(IC+K)=CK
      ERROR=0.0
      DO 11 I=1,M
      R(I)=R(I)+CK*DBLE(ARRAY(I1L1+I))
11    ERROR=ERROR+W(I)*SNGL(R(I)-DBLE(F(I)))**2
      IF(ERROR.GT.ES.AND.EPS.GE.0.0)GO TO 12
      IF(NDEG.EQ.MAXDEG)GO TO 14
      IF(ERROR.LE.TOL.AND.EPS.GE.0.0)GO TO 14
      NDEG=NDEG+1
      K=K+1
      GO TO 8
12    NDEG=NDEG-1
      ERROR=ES
      DO 13 I=1,M
13    R(I)=R(I)-CK*DBLE(ARRAY(I1L1+I))
14    EPS=SQRT(ERROR/RM)
      RETURN
      END
```

*** FUNCTION EVAL ***

```
      FUNCTION EVAL(Y,N,ARRAY,MAXDEG)
      DIMENSION ARRAY(1)
      IB=MAXDEG+1
      IC=MAXDEG+IB-1
      IF(N.GT.0)GO TO 1
      EVAL=ARRAY(IC)
      RETURN
 1    IF(N.GT.1)GO TO 2
      EVAL=ARRAY(IC)+ARRAY(IC+1)*(Y-ARRAY(1))
      RETURN
 2    DKP2=ARRAY(IC+N)
      DKP1=ARRAY(IC+N-1)+(Y-ARRAY(N))*DKP2
      NL2=N-2
      IF(NL2.LT.1)GO TO 4
      DO 3 L=1,NL2
      K=1+NL2-L
      DK=ARRAY(IC+K)+(Y-ARRAY(K+1))*DKP1
     1  -ARRAY(IB+K)*DKP2
      DKP2=DKP1
 3    DKP1=DK
 4    EVAL=ARRAY(IC)+(Y-ARRAY(1))*DKP1
     1  -ARRAY(IB)*DKP2
      RETURN
      END
```

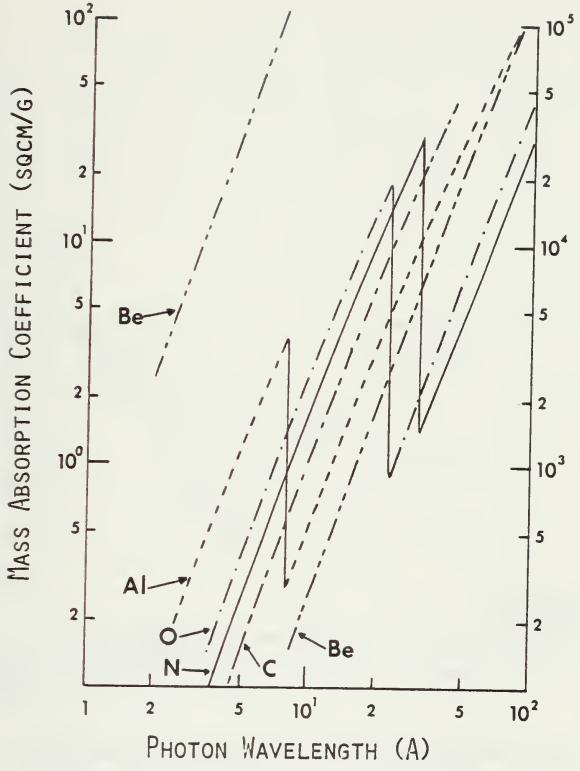

Mass absorption coefficients versus photon wavelength for several absorption filter materials. [15]

FIGURE 1

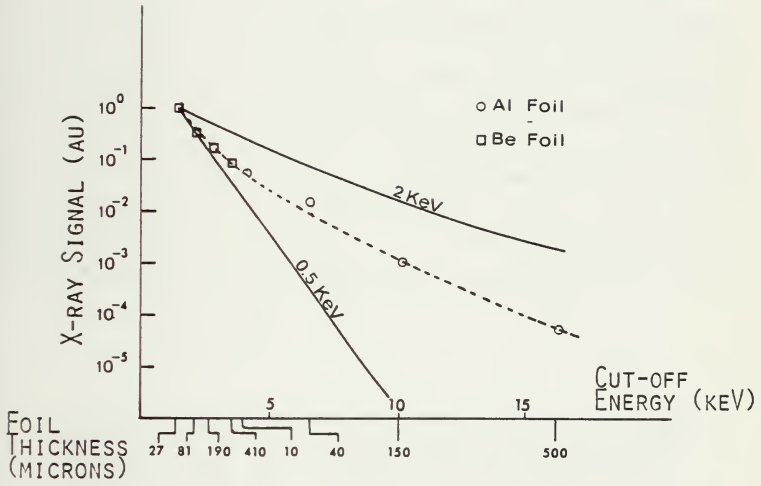

Example of emitted x-ray intensities from a plasma as a function of cut-off energy, E_c, for four Be and four Al foils of different thicknesses. The slope of the dotted line which fits the experimental points is between those for curves of T_e=500eV and T_e=2keV. Laser energy is 20J delivered in 10nsec. [37]

FIGURE 2

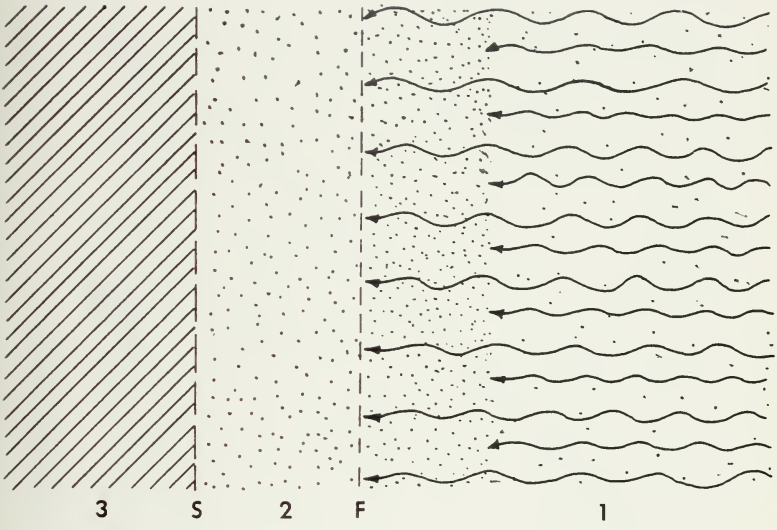

Laser target interaction zones: (1)laser light absorption zone, (2)high density zone, (3)undisturbed solid, (F)electron density equals the critical density, (S)shock front of the compression wave. [18]

FIGURE 3

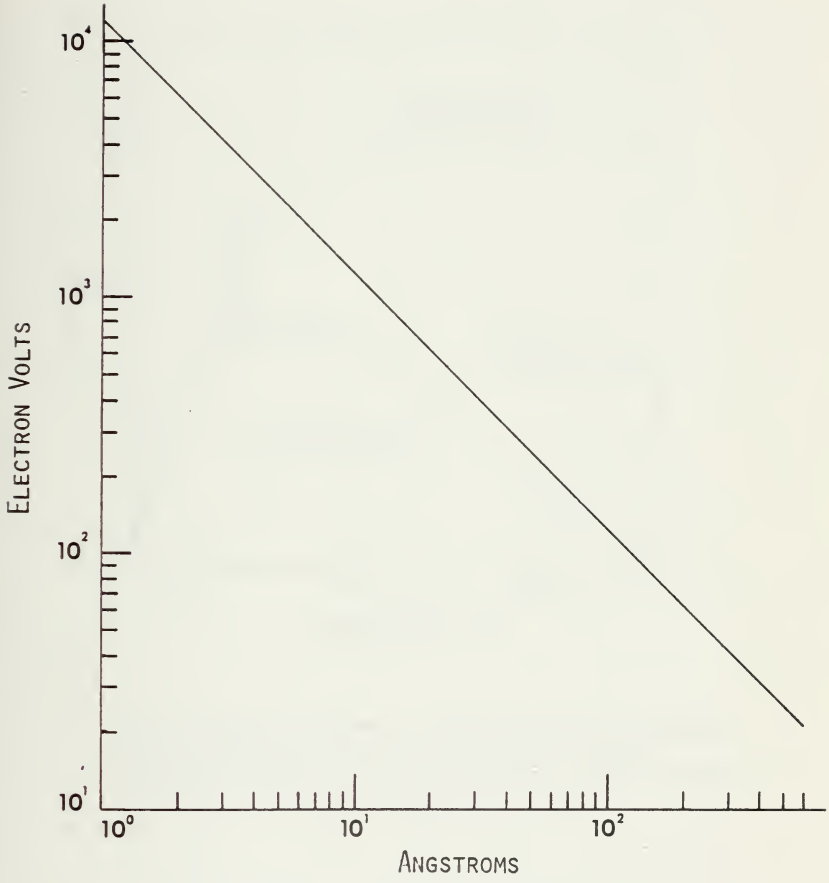

Graph for converting photon energies expressed in Angstroms into electron volts.

FIGURE 4

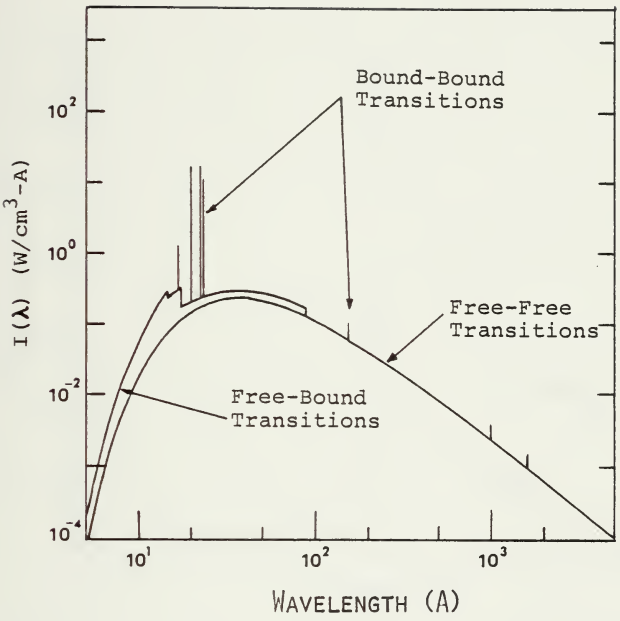

Calculated features of the radiation spectrum of a hydrogen plasma contaminated by 2% oxygen. kT_e=170eV, $N_e=10^{18}cm^{-3}$. Gaunt factor corrections are not included. [29]

FIGURE 5

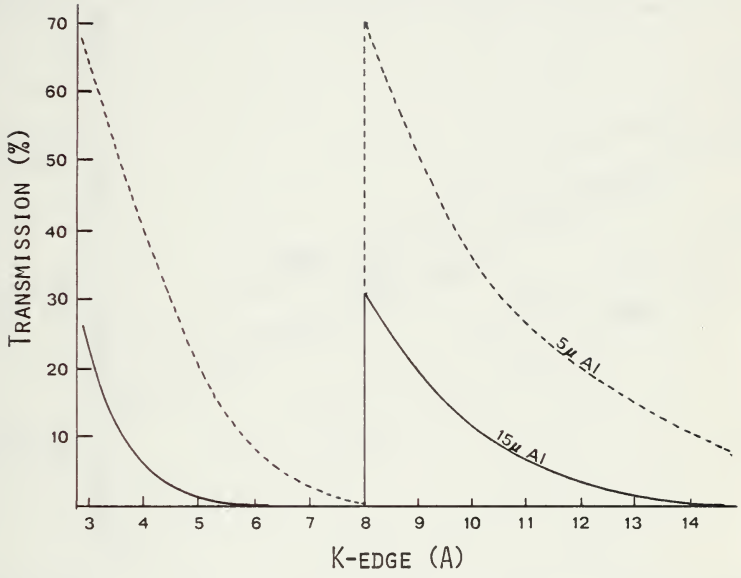

Transmission curve of 5 and 15 micron Al filter. [15]

FIGURE 6

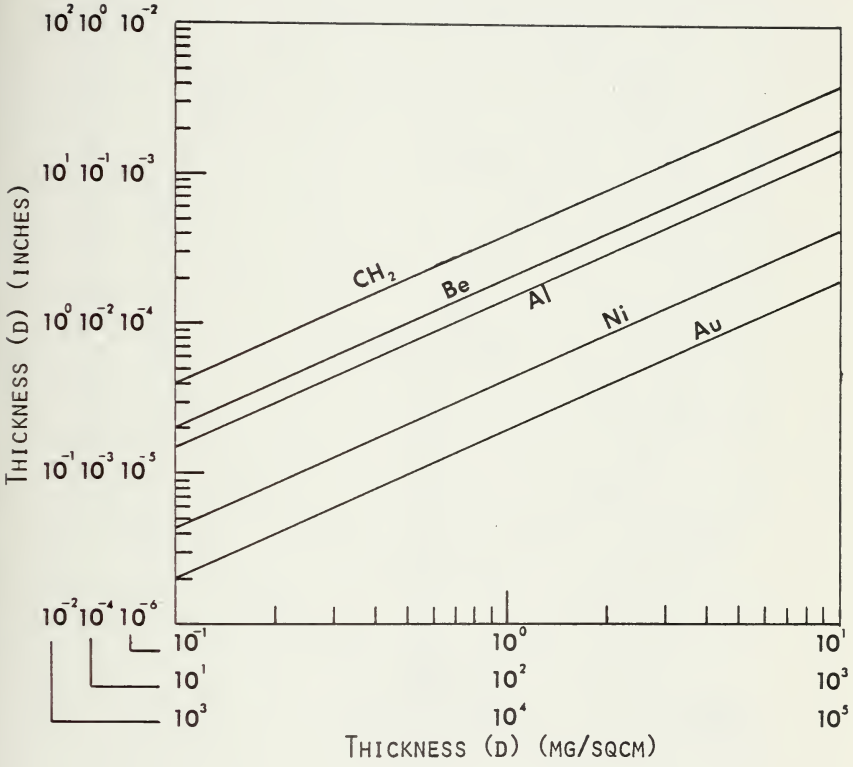

Graph for converting foil thicknesses expressed in mg/sqcm into inches for various foil materials. [7]

FIGURE 7

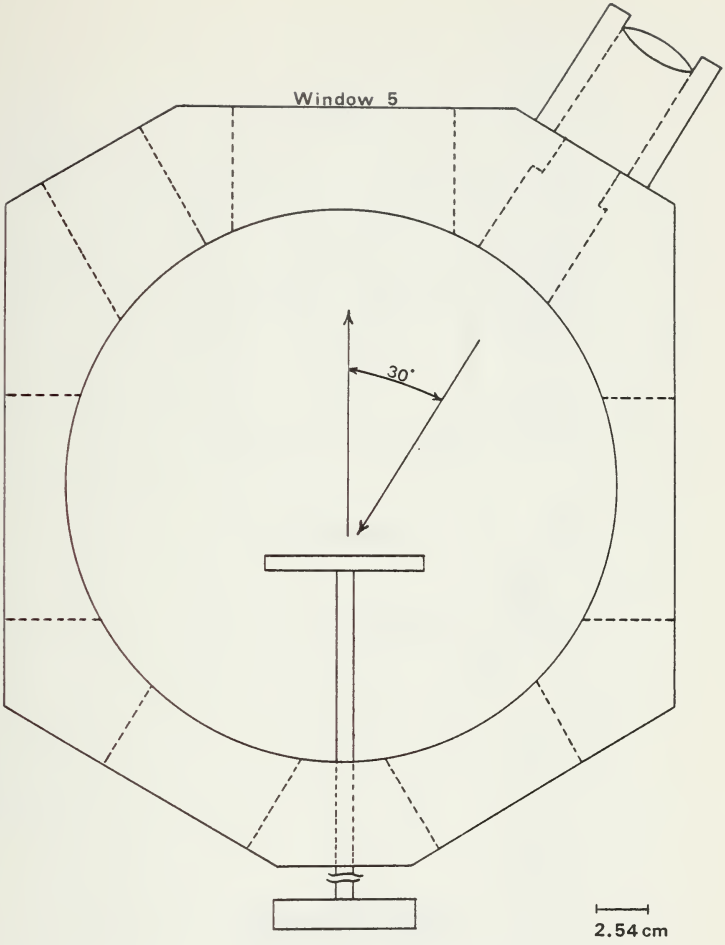

Top view of vacuum chamber.

FIGURE 8

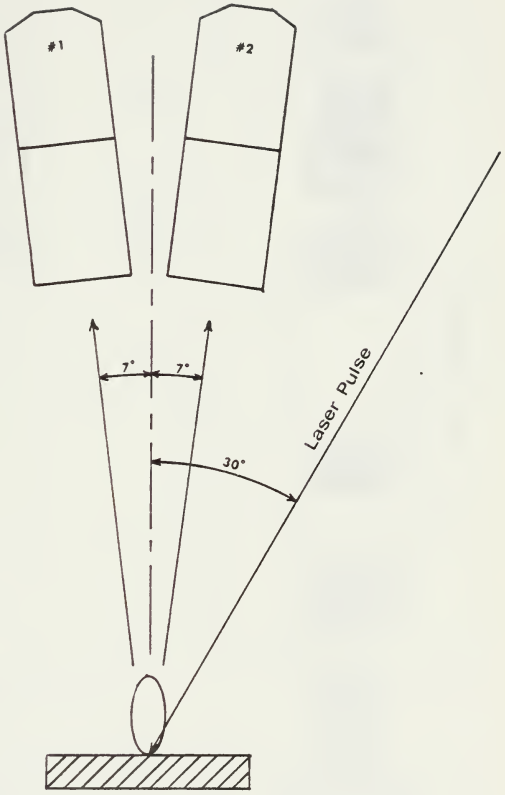

Top view of x-ray probes in relation to the laser pulse, target and the plasma. The laser pulse and probes are located in the horizontal plane.

FIGURE 9

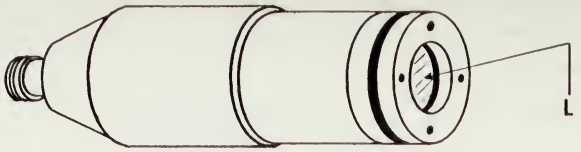

ASSEMBLED PROBE

A. four 0-80 machine screws
B. aperture
C. neoprene gasket (inner)
D. neoprene gasket (outer)
E. filter retaining ring
F. filter holder
G. light shield (front)
H. PIN diode and mount
J. BNC to N-type adapter
K. light shield (rear)
L. metal absorption filter

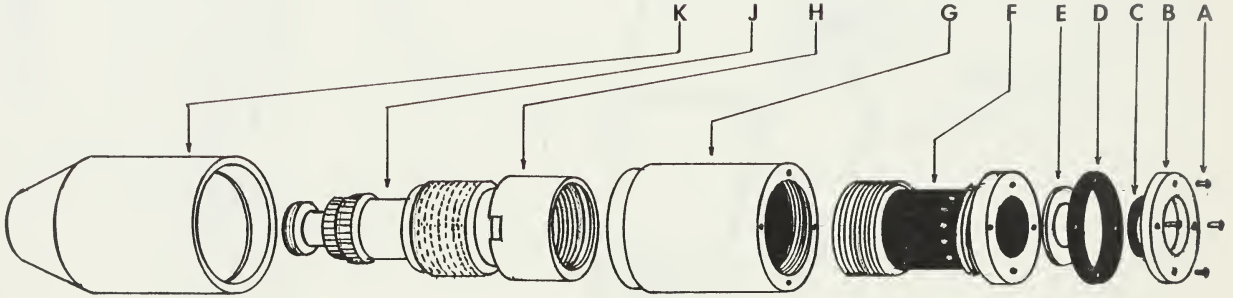

X-RAY PROBE ASSEMBLY

FIGURE 10

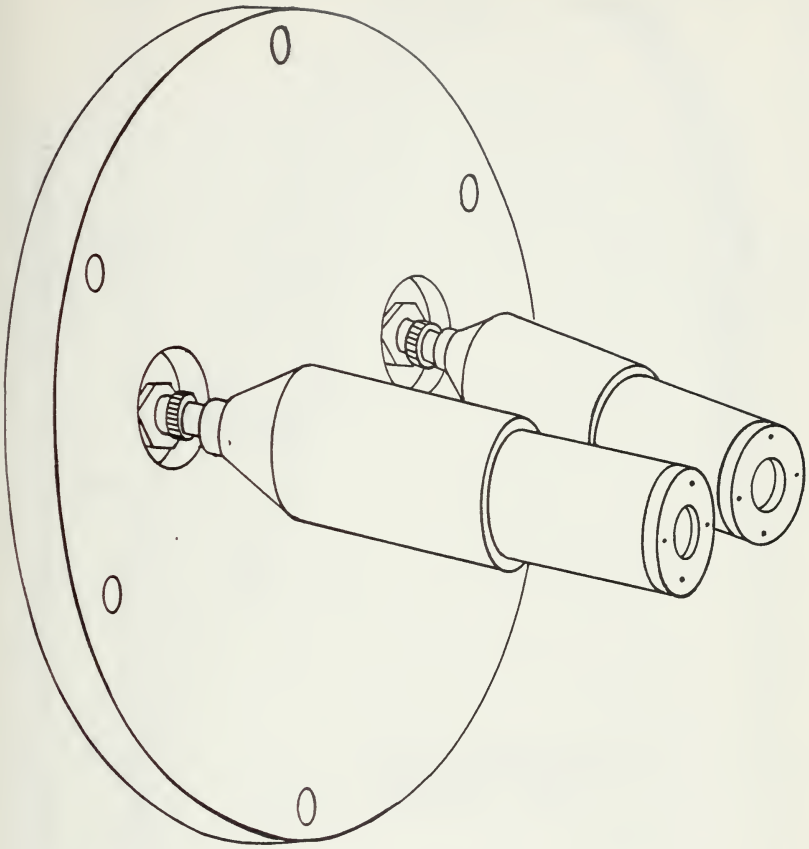

Two x-ray probes mounted on a 5 inch diameter, 1/2 inch thick Aluminum plate. Electrical connections through the plate are made with vacuum tight BNC connectors. The plate forms a vacuum bulkhead in window 5 of the chamber.

FIGURE 11

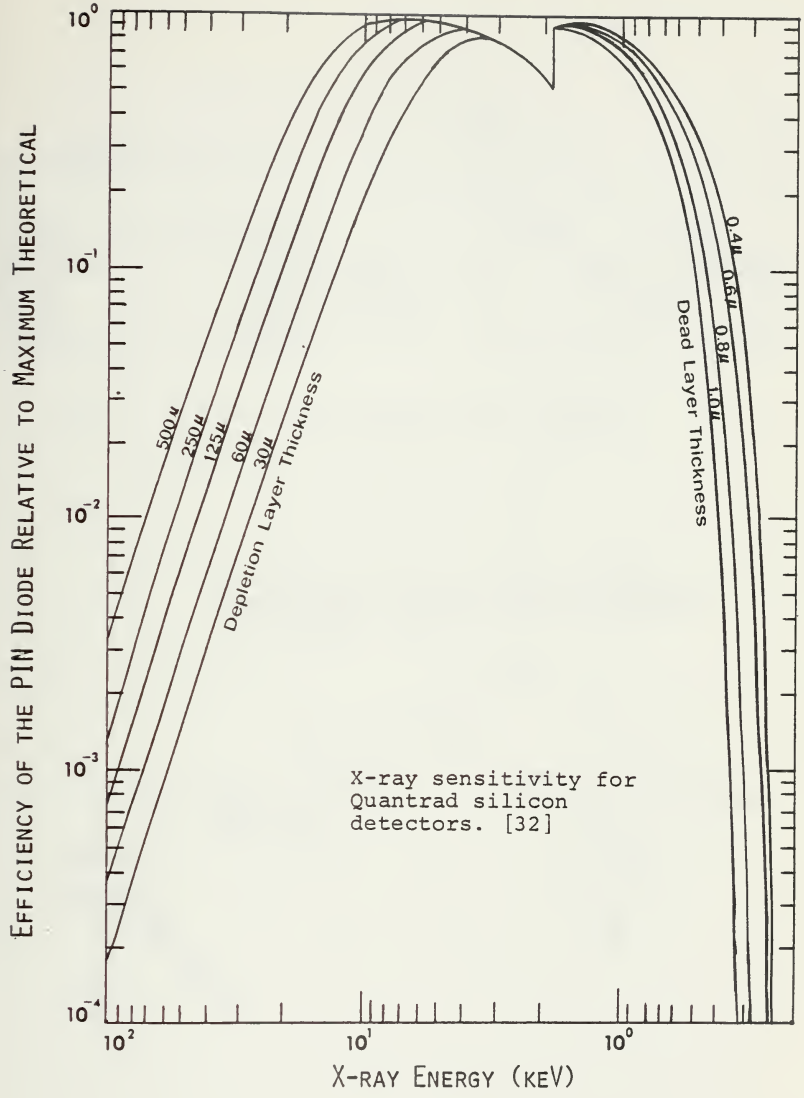
Efficiency of the PIN Diode Relative to Maximum Theoretical
10^0
10^{-1}
10^{-2}
10^{-3}
10^{-4}
500μ
250μ
125μ
60μ
30μ
Depletion Layer Thickness
0.4μ
0.6μ
0.8μ
1.0μ
Dead Layer Thickness
X-ray sensitivity for Quantrad silicon detectors. [32]
10^2
10^1
10^0
X-ray Energy (keV)

FIGURE 12

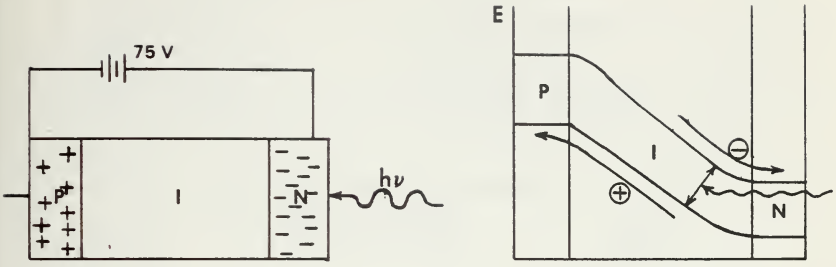

a. PIN diode energy level diagram

b. Schematic diagram of the biasing circuit for a single double diffused PIN silicon diode. [32]

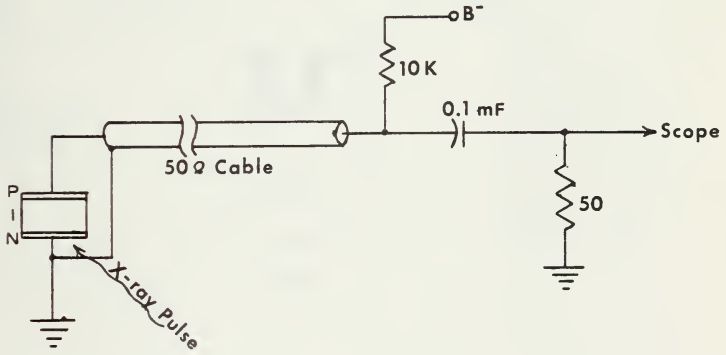

FIGURE 13

A. CW alignment laser
B. Pockels cell
C. Polarizer
D. Nd oscillator
E. Beam expansion optics
F. Nd amplifier
G. Beam splitter
H. K-D1 photodiode
J. MgO diffuser
K. Trigger diode
L. +3 diopter converging lens
M. Tek 564B storage scope
N. Energy signal
P. X-ray probes
Q. Target
R. Vacuum chamber
S. Delay cable
T. Delay box
U. DC bias voltage
V. Biasing circuit
W. Inverting transformer
X. Tek 7904 scope
Y. Laser power and trigger signal

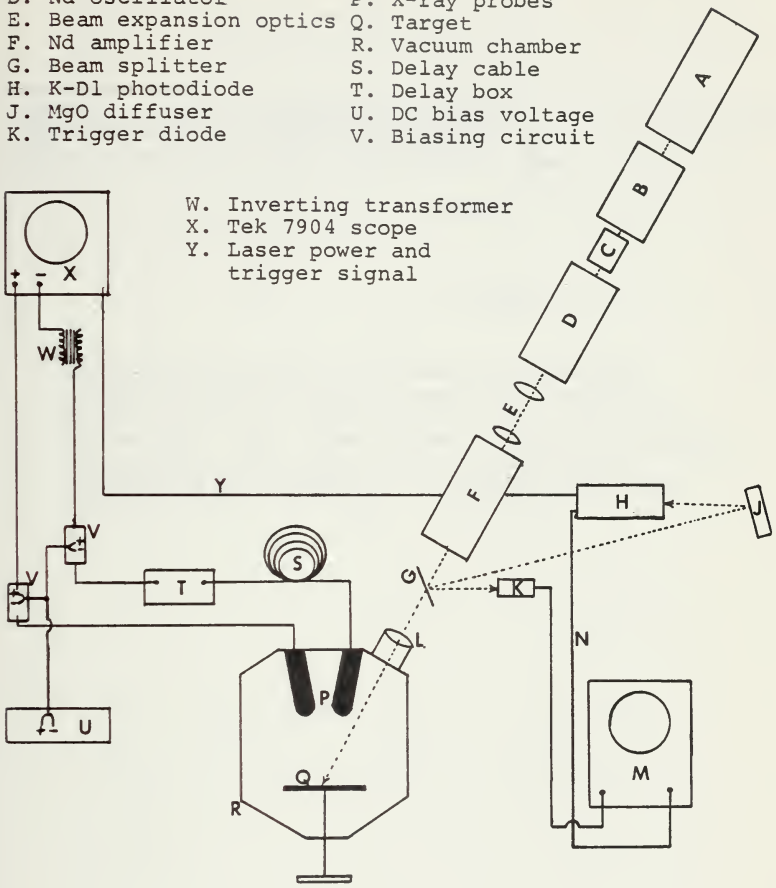

FIGURE 14

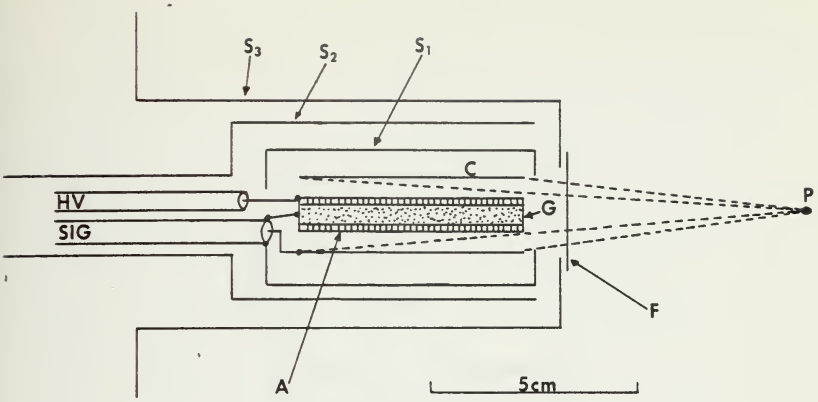

Schematic diagram of the Vacuum Photodiode constructed at the NPS Plasma Facility: (S_3) screen at vacuum chamber potential, (S_2) floating screen, (S_1) inner screen at ground potential, (C) cathode, (G) grounded core of the anode, (F) absorption foil window, (P) plasma, (HV) high voltage lead, (SIG) signal lead. [16]

FIGURE 15

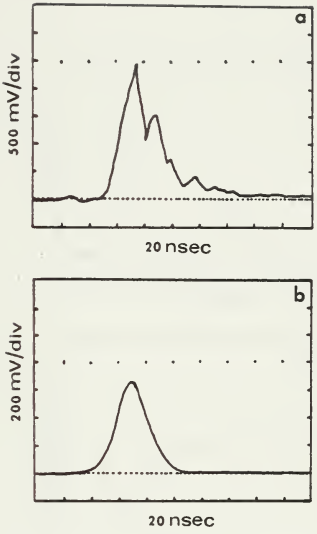

Vacuum Photodiode signal: (a)X-ray signal passing through 1.83mg/sqcm Aluminum foil with a 10.7J laser pulse and Aluminum target. (b)Simultaneously recorded laser pulse.

FIGURE 16

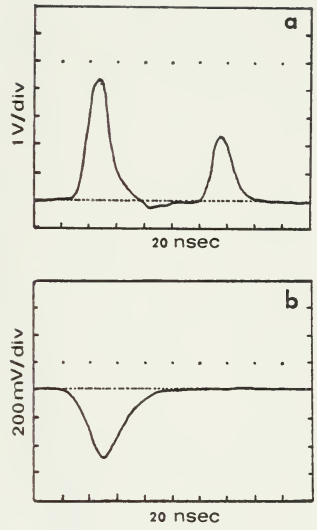

Typical temperature data from x-ray probes 1 and 2: (a)X-ray signal of probe 1 through Aluminum foil of thickness 3.66mg/sqcm followed by a delayed signal from probe 2 through Aluminum foil of thickness 4.30mg/sqcm. (b)Simultaneously recorded laser pulse of 9.0J, FWHM 25nsec.

FIGURE 17

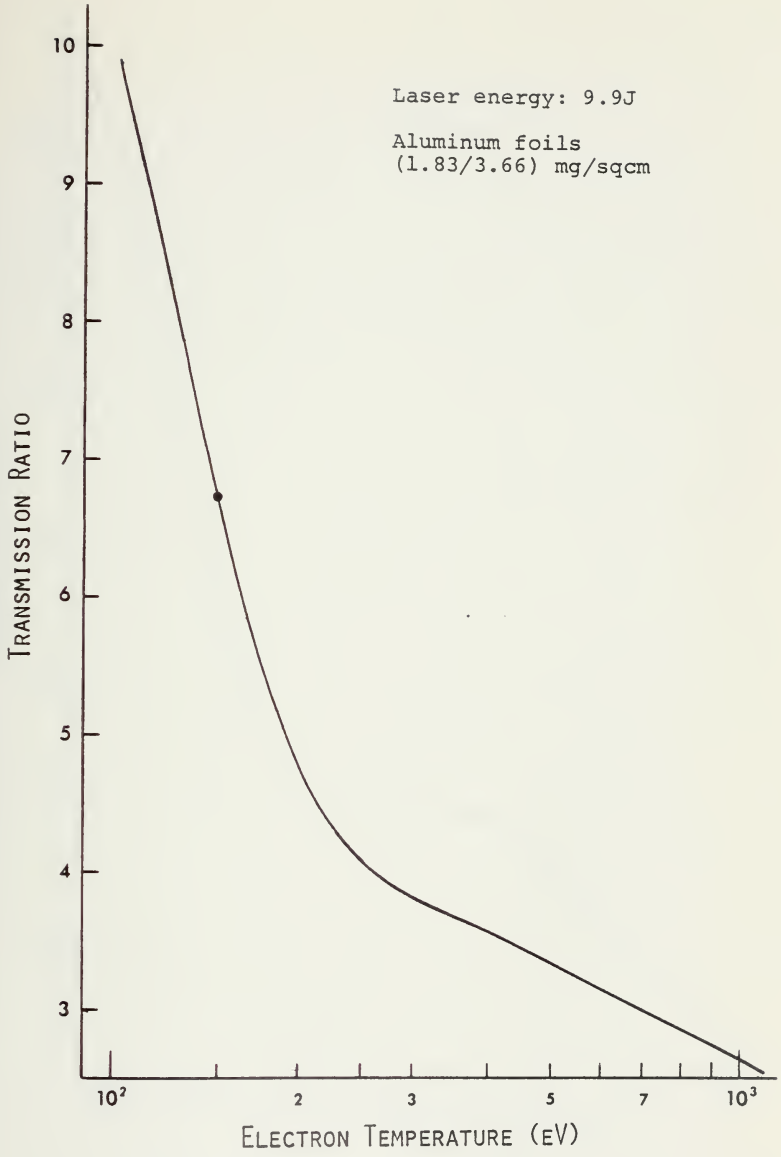
Laser energy: 9.9J
Aluminum foils
(1.83/3.66) mg/sqcm
Transmission Ratio
10
9
8
7
6
5
4
3
10^2
2
3
5
7
10^3
Electron Temperature (eV)

FIGURE 18


Laser energy: 9.9J
Aluminum foils
(3.66/5.50) mg/sqcm
5.5
5
4.5
4
3.5
3
2.5
TRANSMISSION RATIO
10^2
2
3
5
7
10^3
ELECTRON TEMPERATURE (EV)

FIGURE 19

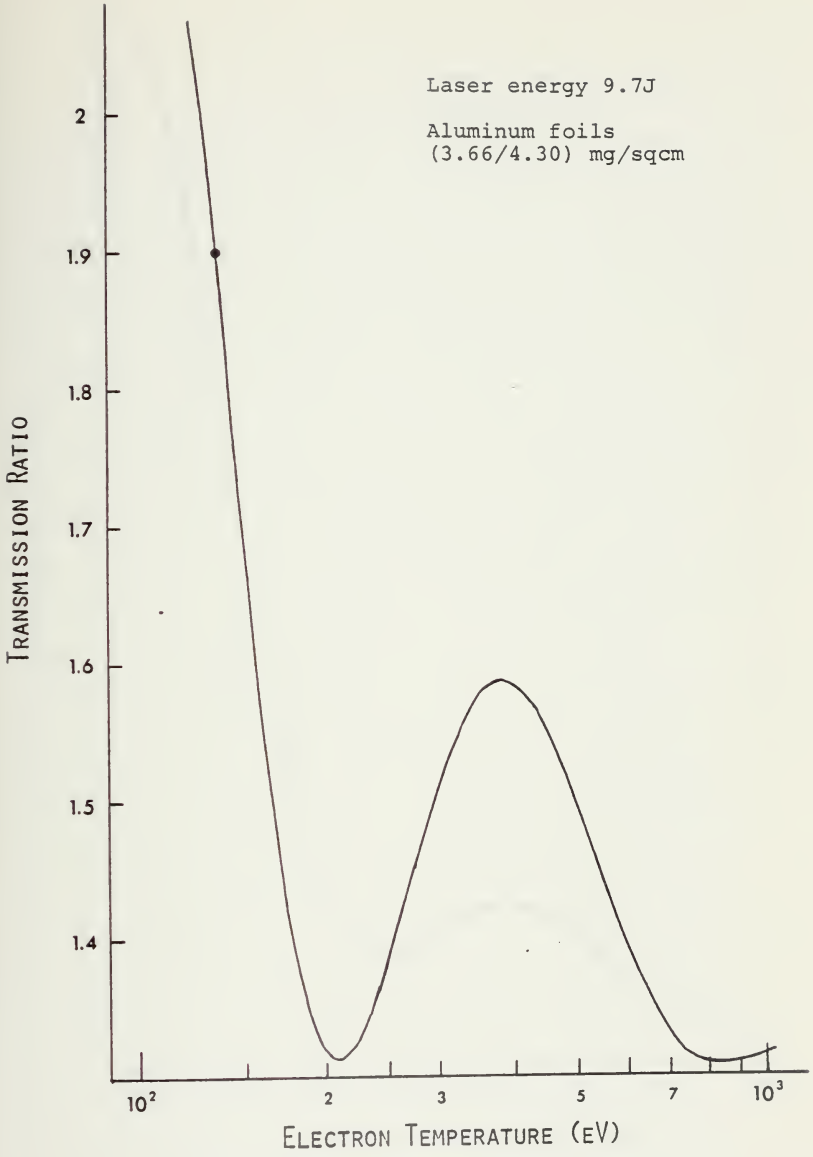
Laser energy 9.7J
Aluminum foils
(3.66/4.30) mg/sqcm
2
1.9
1.8
1.7
1.6
1.5
1.4
TRANSMISSION RATIO
10^2
2
3
5
7
10^3
ELECTRON TEMPERATURE (EV)

FIGURE 20

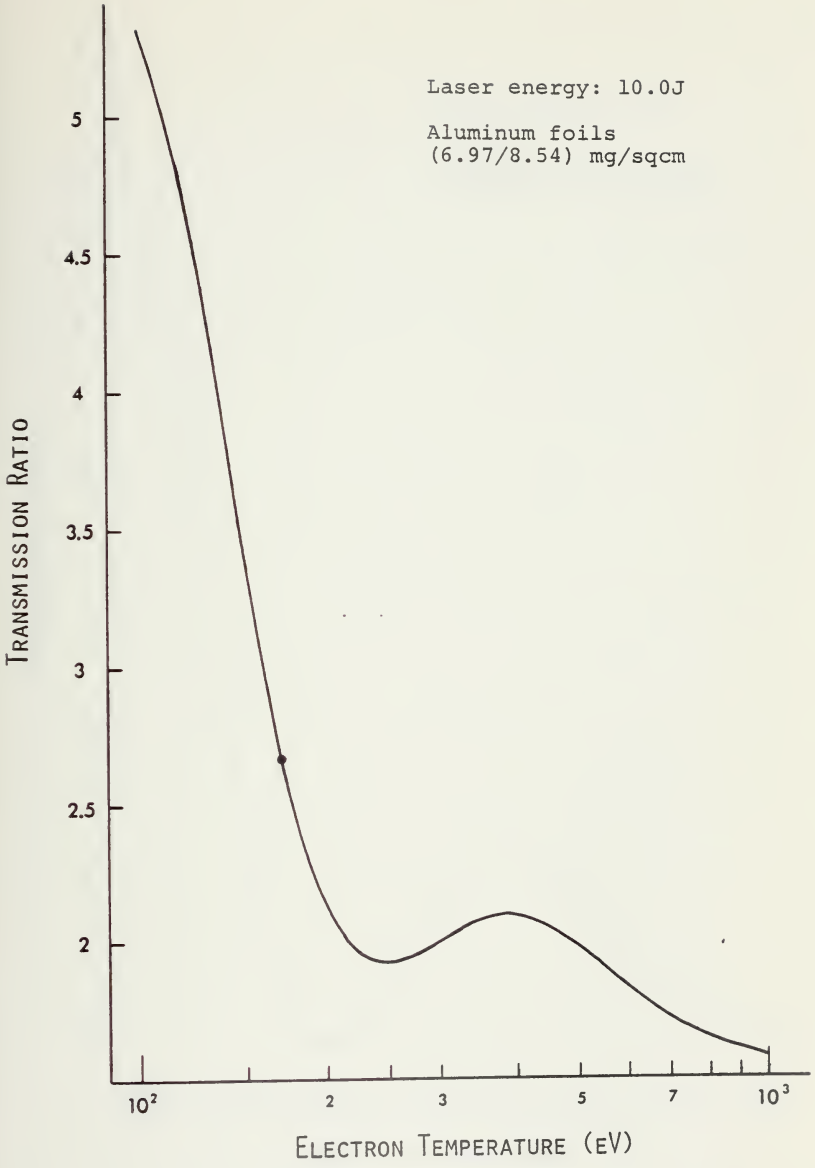
Laser energy: 10.0J
Aluminum foils
(6.97/8.54) mg/sqcm
Transmission Ratio
5
4.5
4
3.5
3
2.5
2
10^2
2
3
5
7
10^3
Electron Temperature (eV)

FIGURE 21

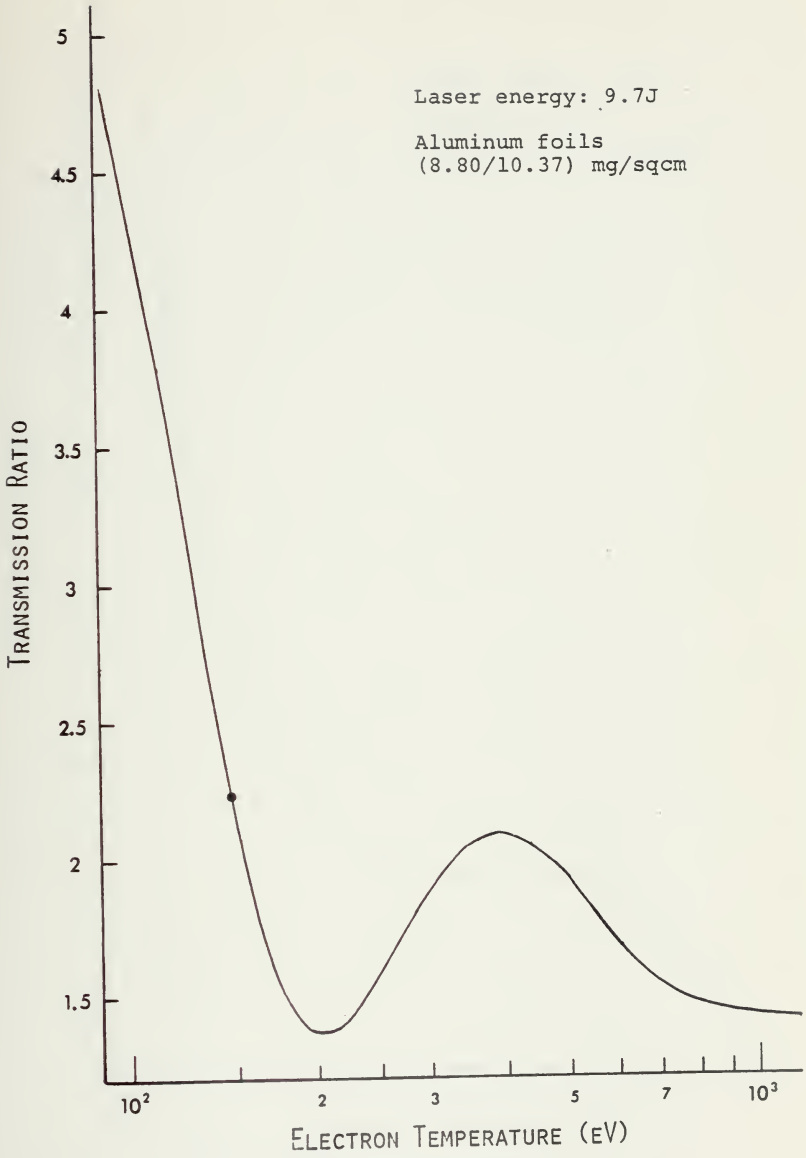
Laser energy: 9.7J
Aluminum foils
(8.80/10.37) mg/sqcm
TRANSMISSION RATIO
5
4.5
4
3.5
3
2.5
2
1.5
10^2
2
3
5
7
10^3
ELECTRON TEMPERATURE (EV)

FIGURE 22

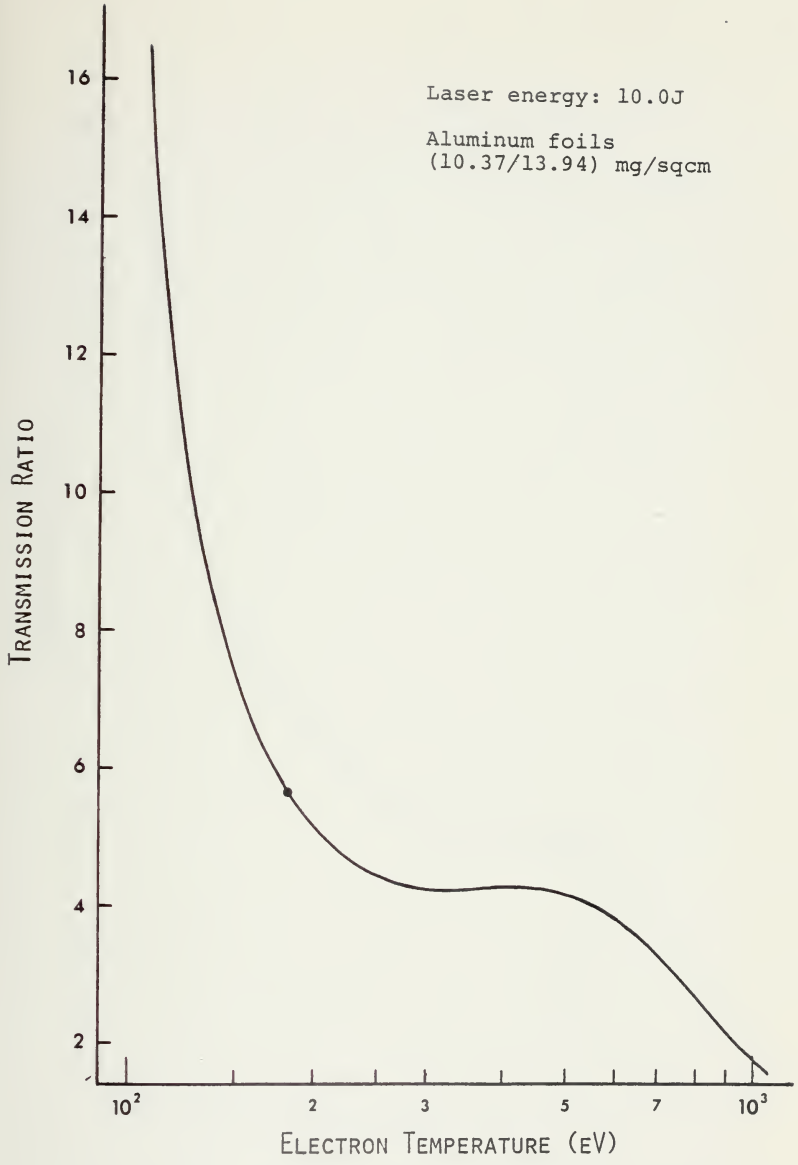
Laser energy: 10.0J
Aluminum foils
(10.37/13.94) mg/sqcm
16
14
12
10
8
6
4
2
Transmission Ratio
10^2
2
3
5
7
10^3
Electron Temperature (eV)

FIGURE 23

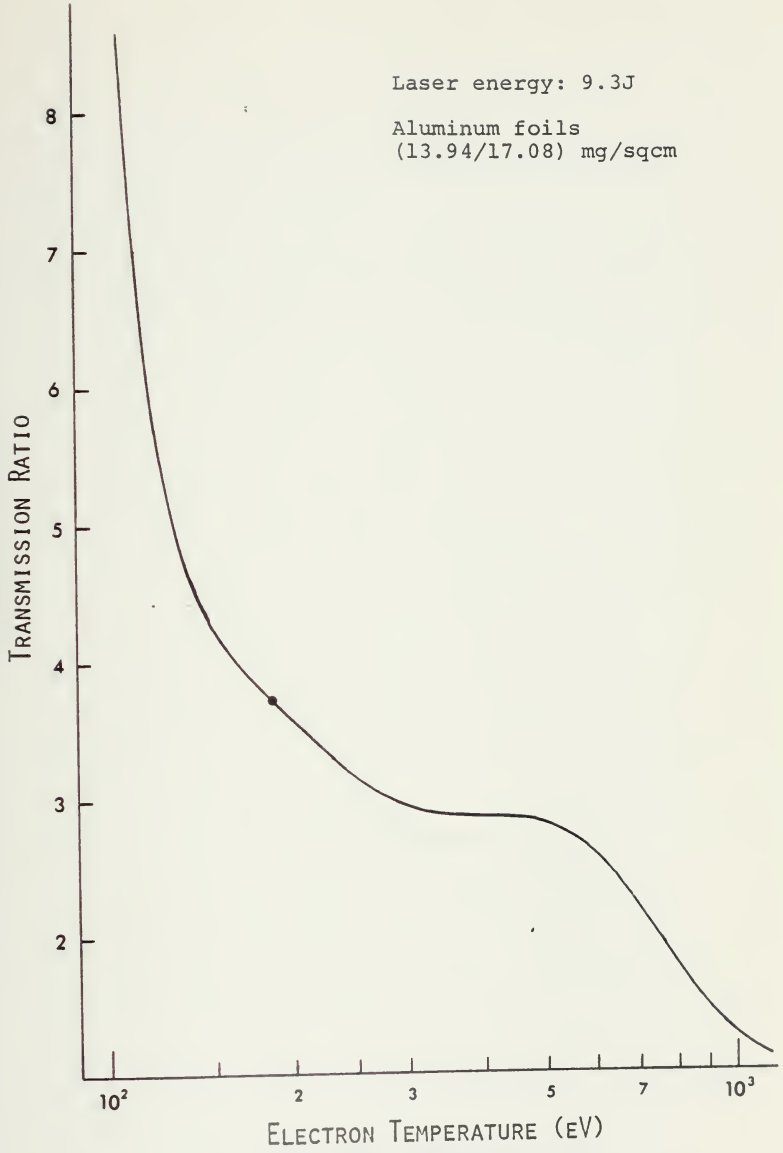
Laser energy: 9.3J
Aluminum foils
(13.94/17.08) mg/sqcm
TRANSMISSION RATIO
8
7
6
5
4
3
2
10^2
2
3
5
7
10^3
ELECTRON TEMPERATURE (EV)

FIGURE 24

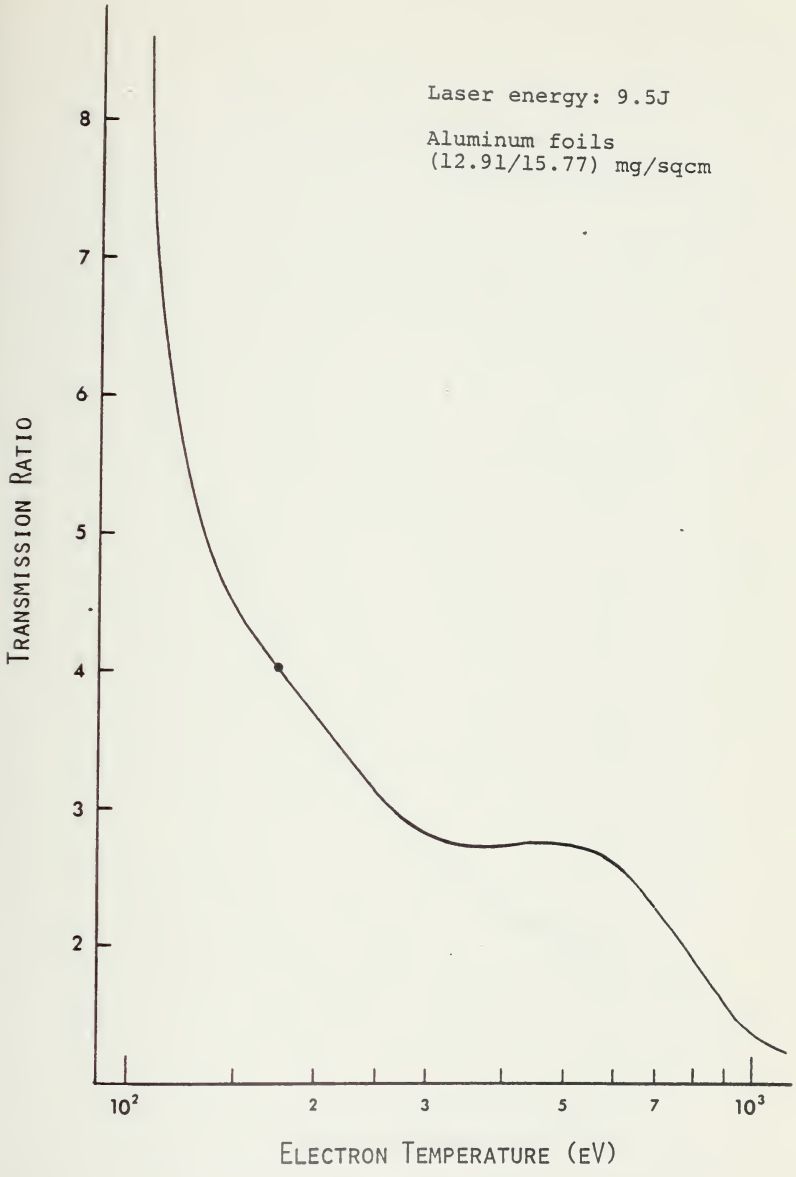
Laser energy: 9.5J
Aluminum foils
(12.91/15.77) mg/sqcm
TRANSMISSION RATIO
8
7
6
5
4
3
2
10^2
2
3
5
7
10^3
ELECTRON TEMPERATURE (eV)

FIGURE 25

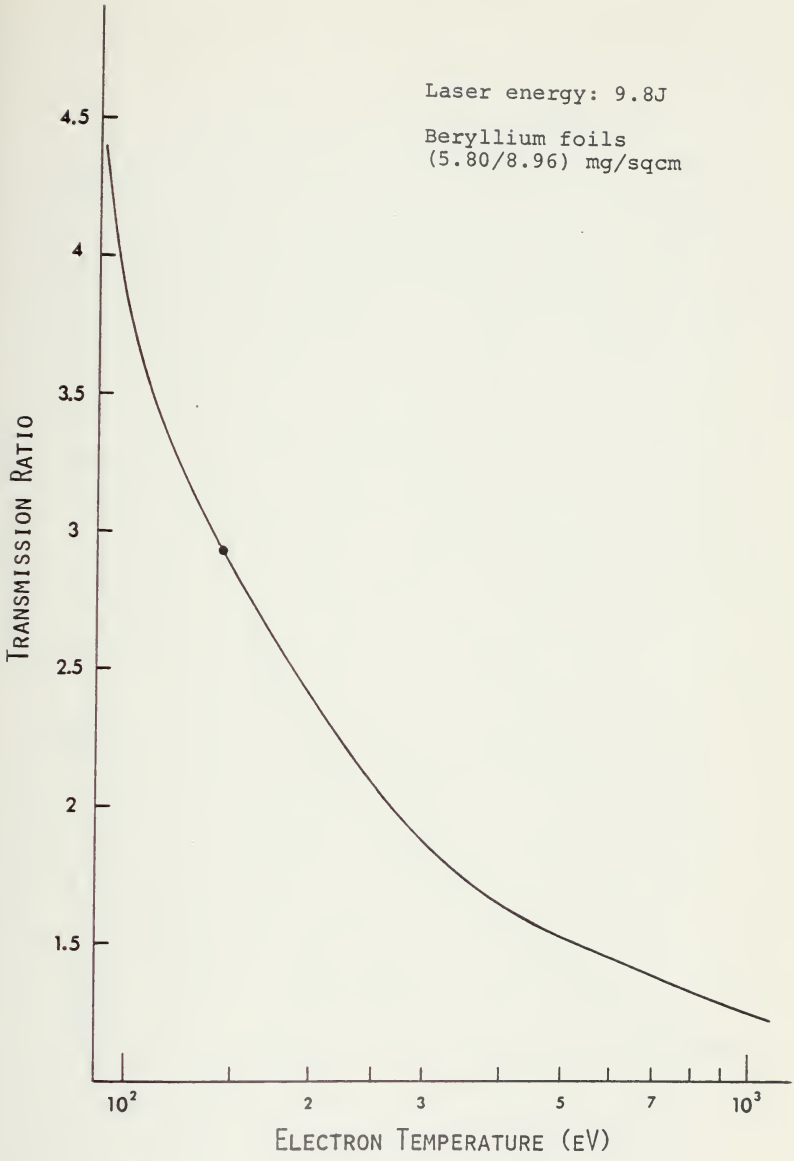
Laser energy: 9.8J
Beryllium foils
(5.80/8.96) mg/sqcm
4.5
4
3.5
3
2.5
2
1.5
TRANSMISSION RATIO
10^2
2
3
5
7
10^3
ELECTRON TEMPERATURE (eV)

FIGURE 26

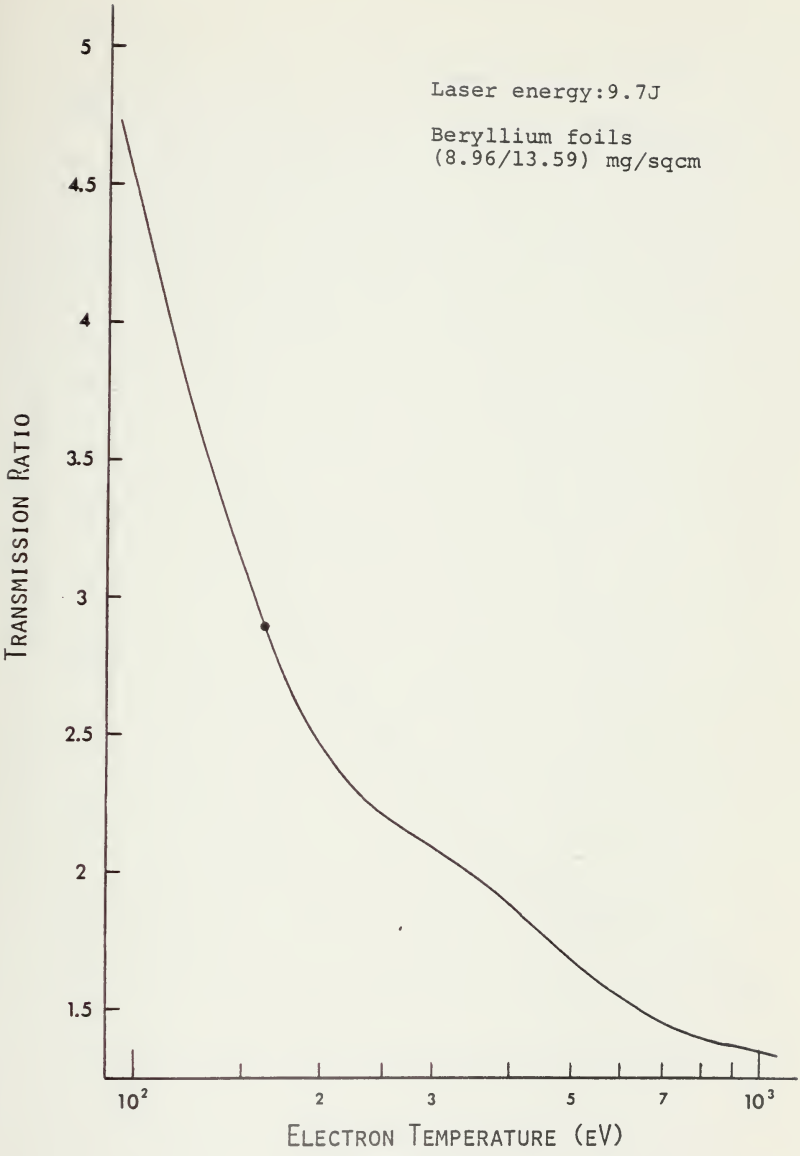
Laser energy:9.7J
Beryllium foils
(8.96/13.59) mg/sqcm
Transmission Ratio
5
4.5
4
3.5
3
2.5
2
1.5
10^2
2
3
5
7
10^3
Electron Temperature (eV)

FIGURE 27

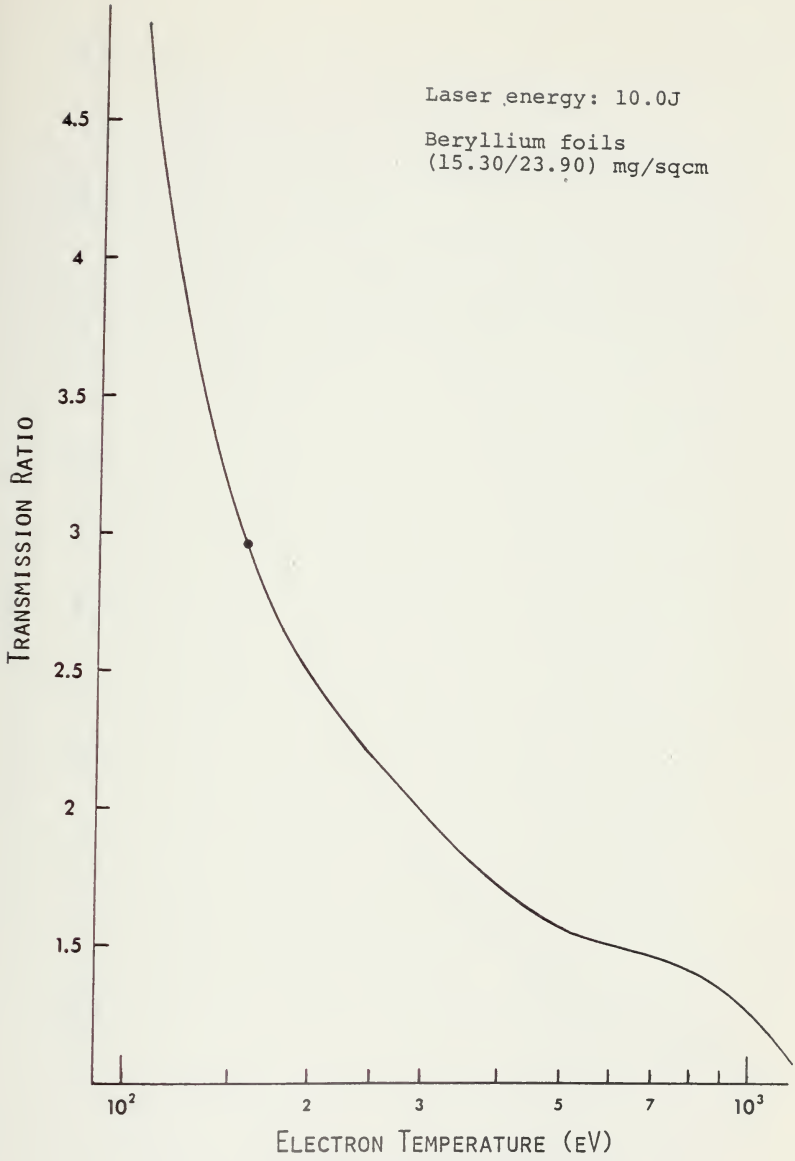
Laser energy: 10.0J
Beryllium foils
(15.30/23.90) mg/sqcm
Transmission Ratio
4.5
4
3.5
3
2.5
2
1.5
10^2
2
3
5
7
10^3
Electron Temperature (eV)

FIGURE 28

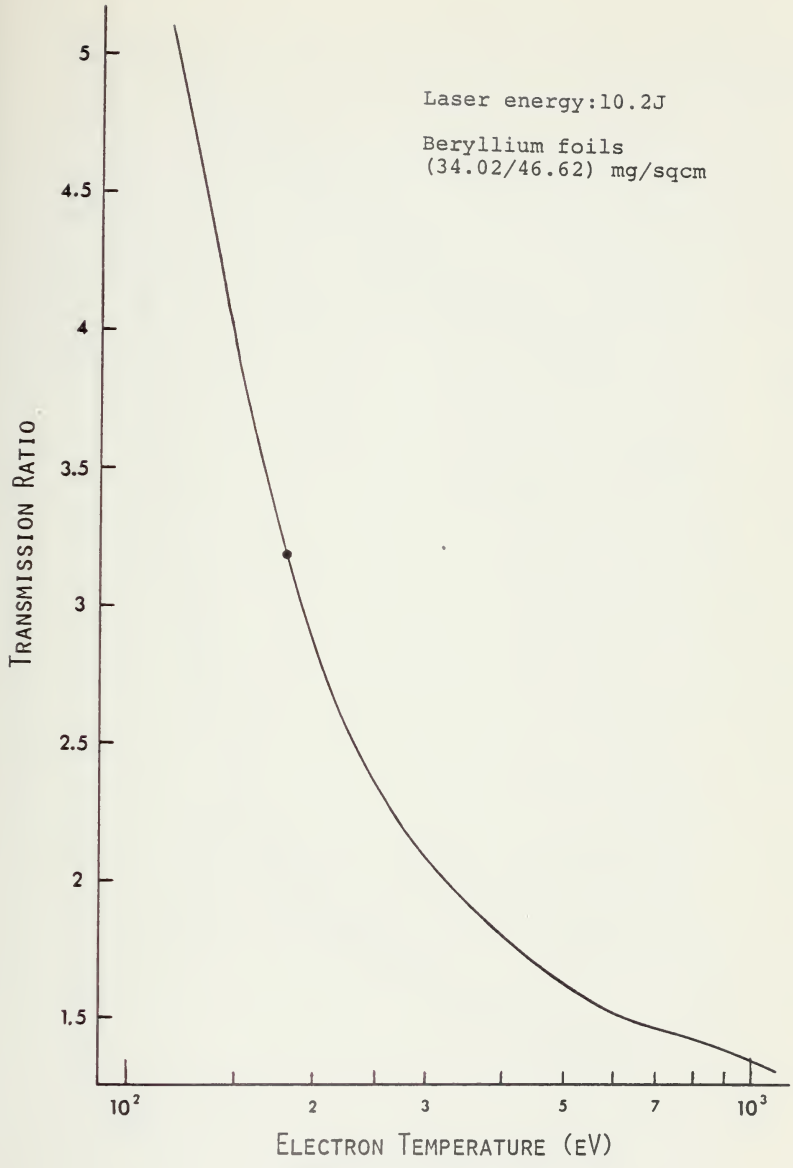
Laser energy:10.2J
Beryllium foils
(34.02/46.62) mg/sqcm
Transmission Ratio
5
4.5
4
3.5
3
2.5
2
1.5
10^2
2
3
5
7
10^3
Electron Temperature (eV)

FIGURE 29

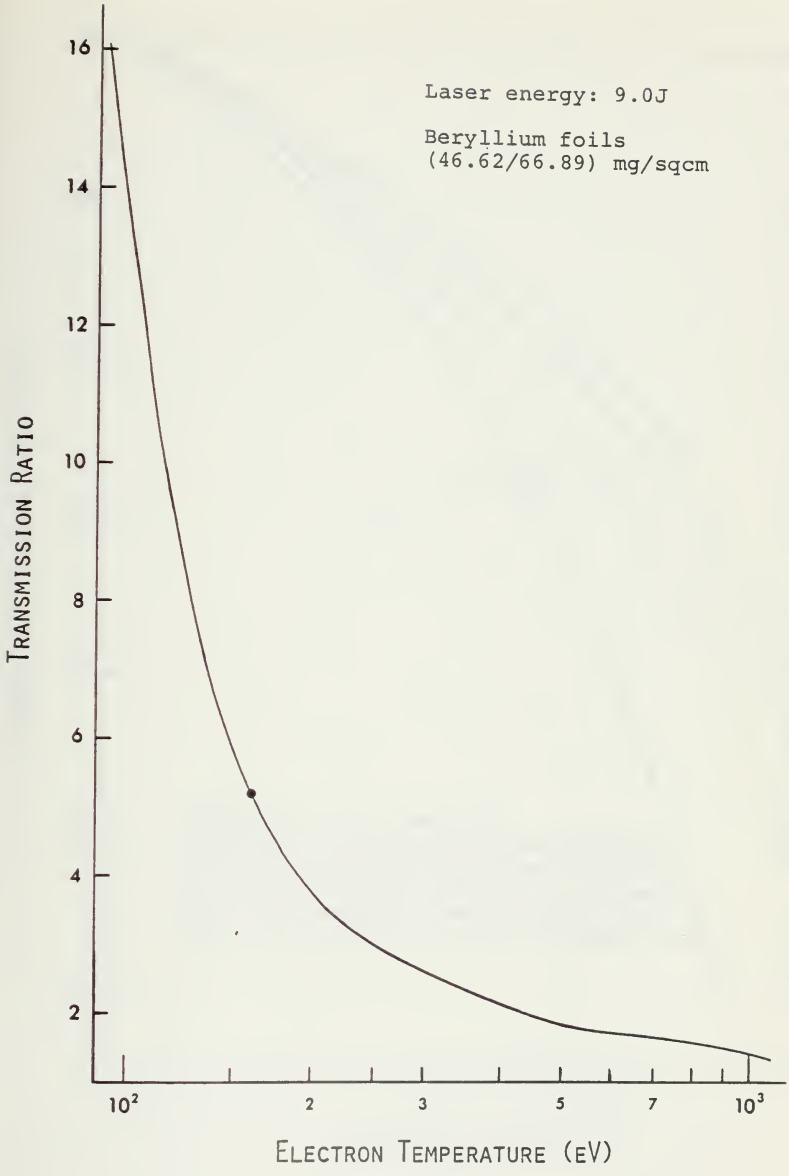
Laser energy: 9.0J
Beryllium foils
(46.62/66.89) mg/sqcm
16
14
12
10
8
6
4
2
Transmission Ratio
10^2
2
3
5
7
10^3
Electron Temperature (eV)

FIGURE 30

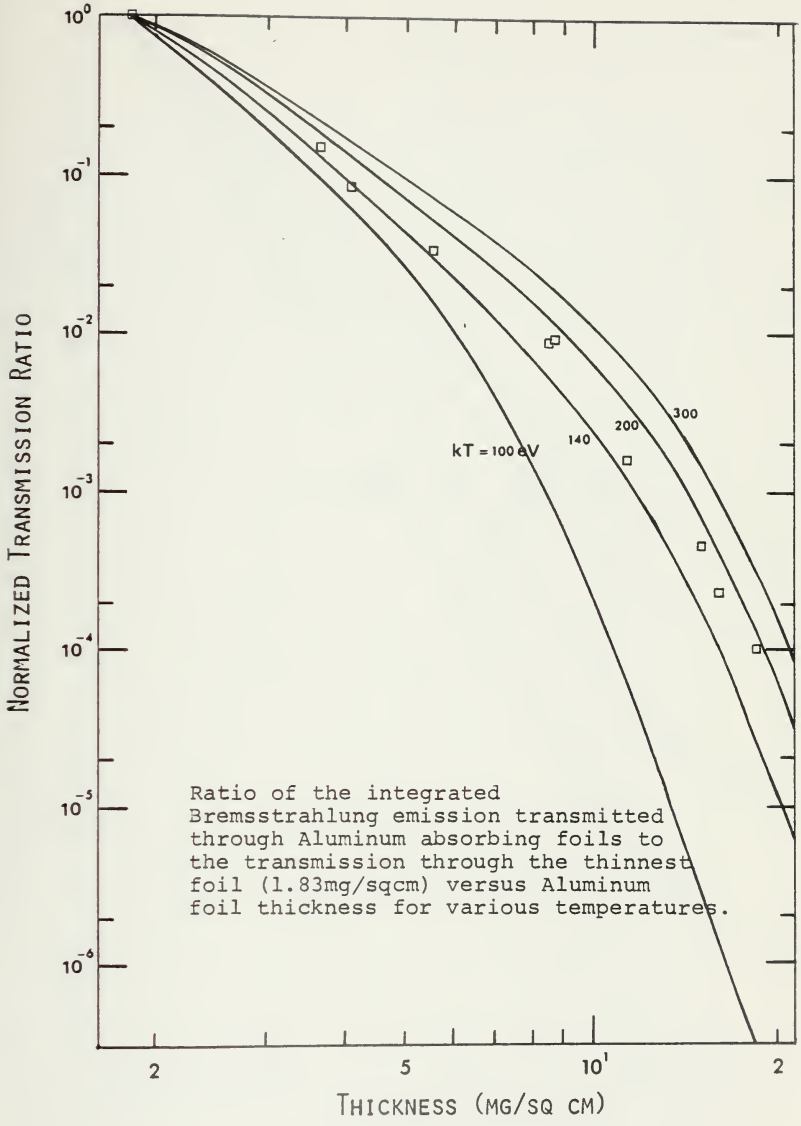
NORMALIZED TRANSMISSION RATIO
10^{0}
10^{-1}
10^{-2}
10^{-3}
10^{-4}
10^{-5}
10^{-6}
kT = 100 eV
140
200
300
Ratio of the integrated Bremsstrahlung emission transmitted through Aluminum absorbing foils to the transmission through the thinnest foil (1.83mg/sqcm) versus Aluminum foil thickness for various temperatures.
2
5
10^{1}
2
THICKNESS (MG/SQ CM)

FIGURE 31

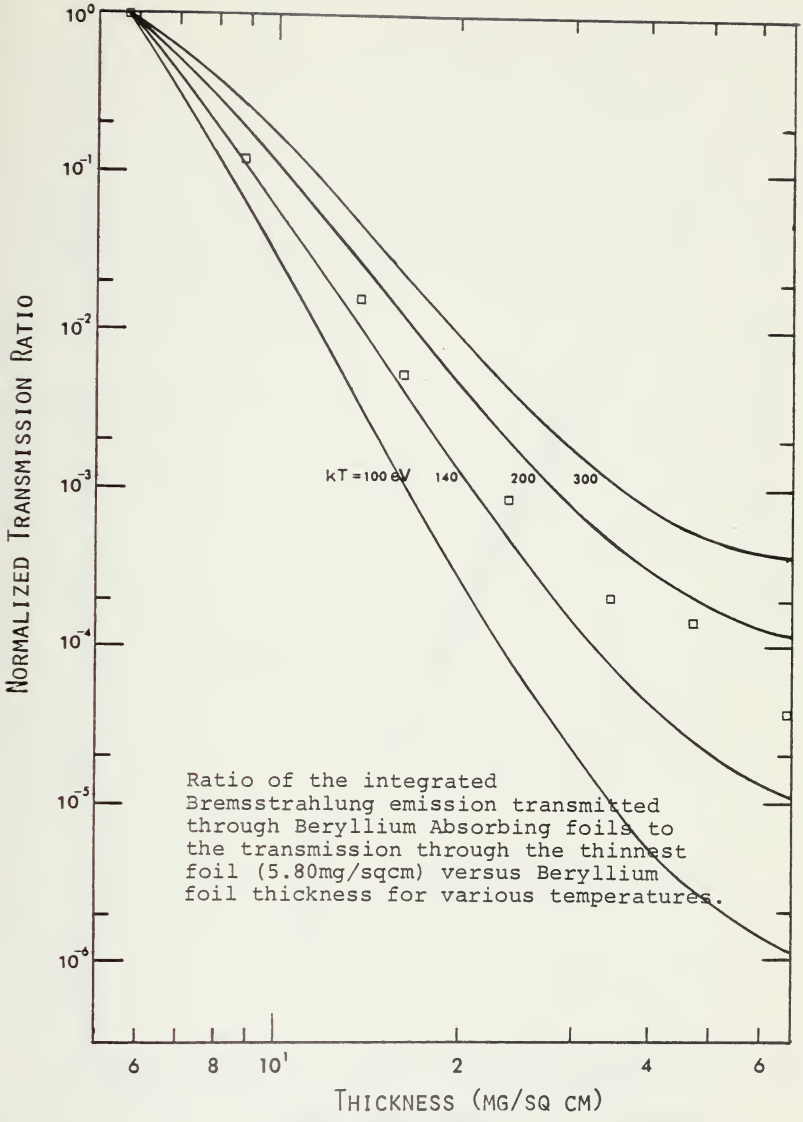
NORMALIZED TRANSMISSION RATIO
10^{0}
10^{-1}
10^{-2}
10^{-3}
10^{-4}
10^{-5}
10^{-6}
kT = 100 eV
140
200
300
Ratio of the integrated Bremsstrahlung emission transmitted through Beryllium Absorbing foils to the transmission through the thinnest foil (5.80mg/sqcm) versus Beryllium foil thickness for various temperatures.
6
8
10^{1}
2
4
6
THICKNESS (MG/SQ CM)

FIGURE 32

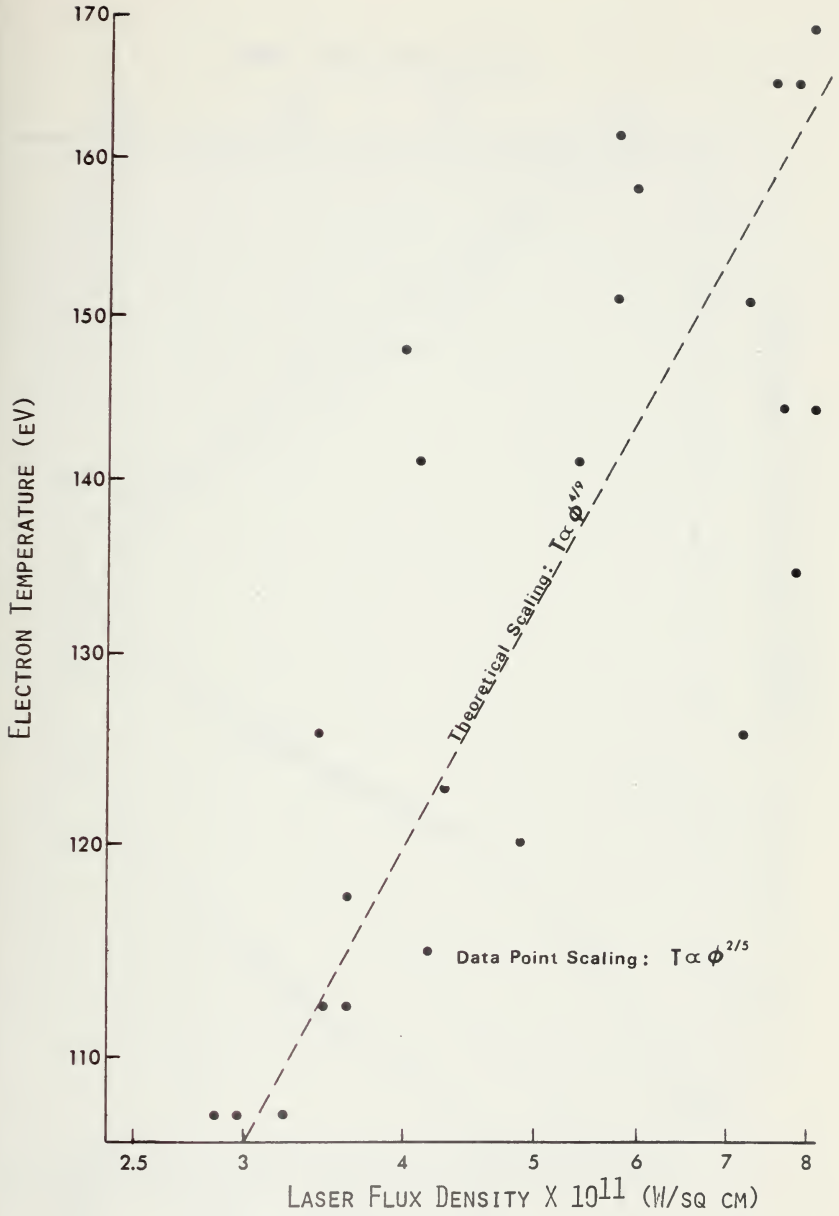
170
160
150
140
130
120
110
Electron Temperature (eV)
Theoretical Scaling: $I \propto \phi^{4/9}$
Data Point Scaling: $I \propto \phi^{2/5}$
2.5
3
4
5
6
7
8
Laser Flux Density X 10^{11} (W/sq cm)

FIGURE 33

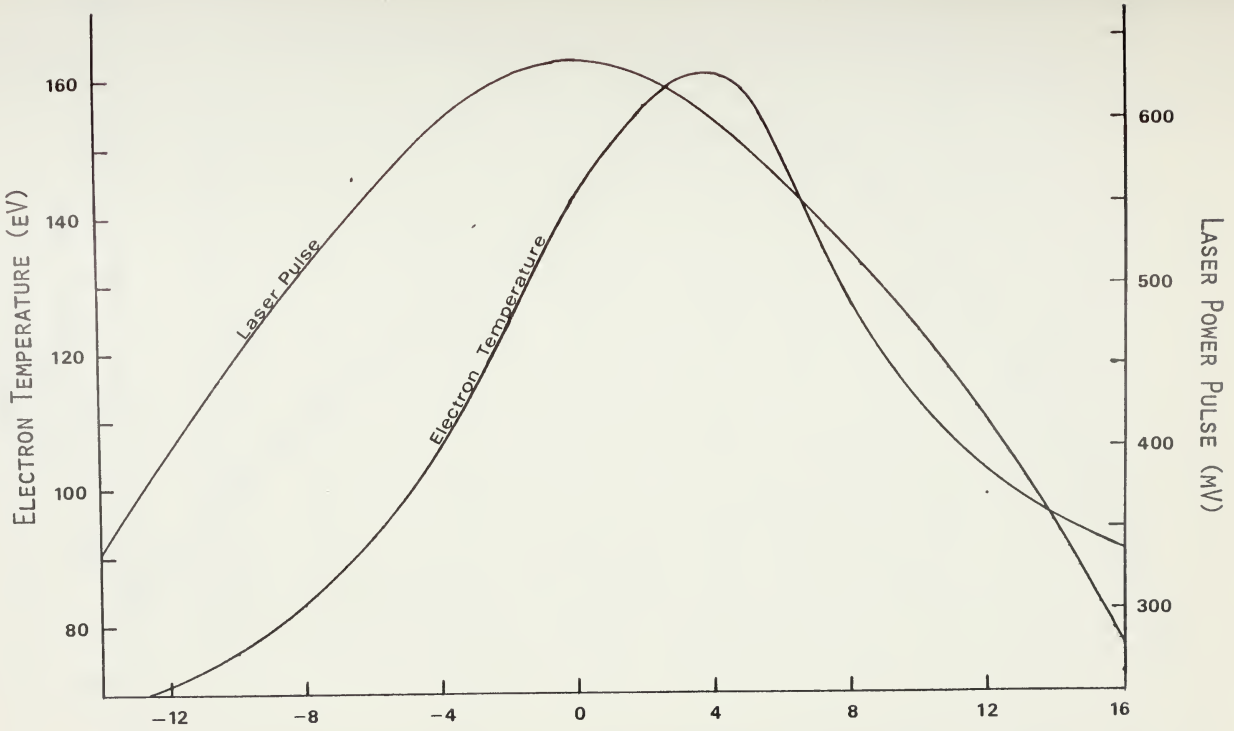
Electron Temperature (eV)
160
140
120
100
80
Laser Pulse
Electron Temperature
600
500
400
300
Laser Power Pulse (mV)
−12
−8
−4
0
4
8
12
16
Time in Nanoseconds Measured from Peak of Laser Pulse

FIGURE 34

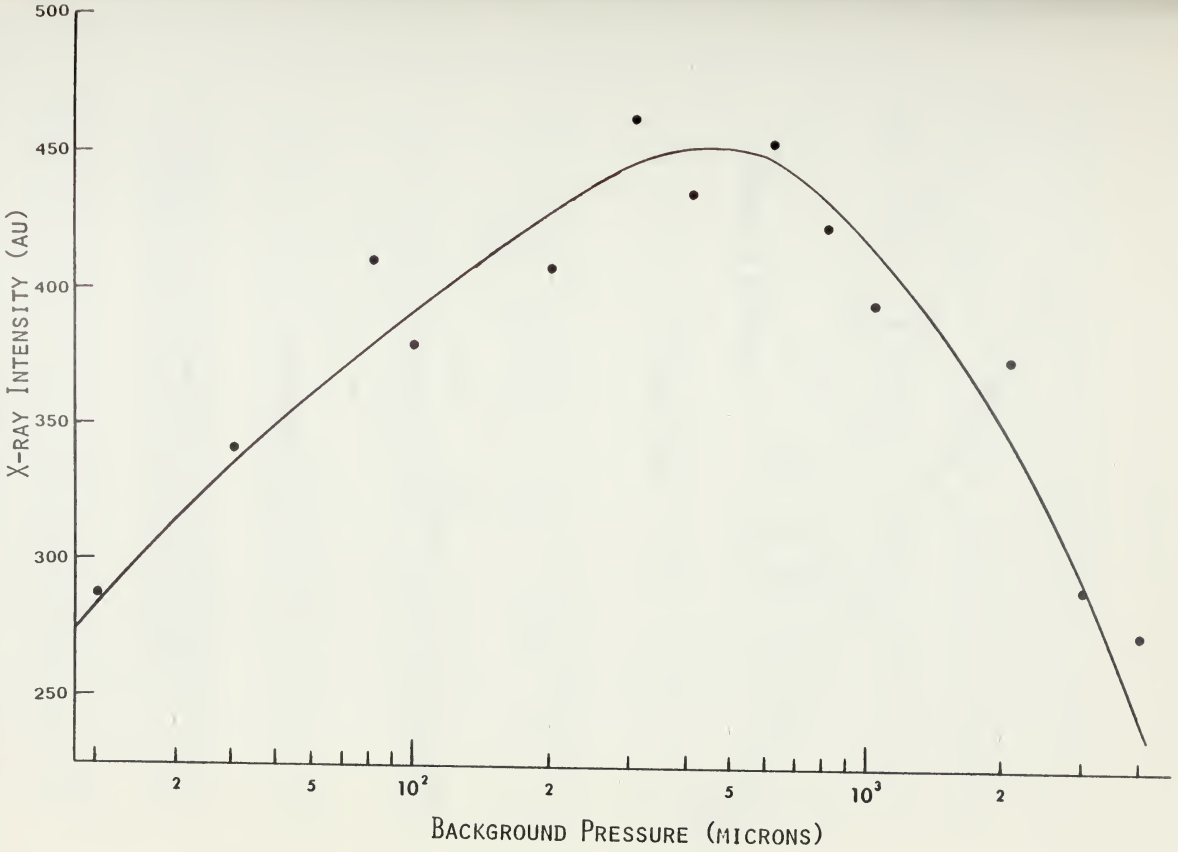
500
450
400
350
300
250
X-RAY INTENSITY (AU)
2
5
10^2
2
5
10^3
2
BACKGROUND PRESSURE (MICRONS)

FIGURE 35

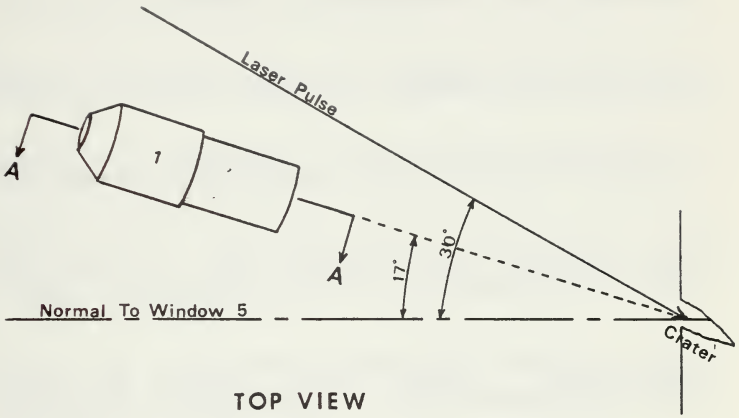

TOP VIEW

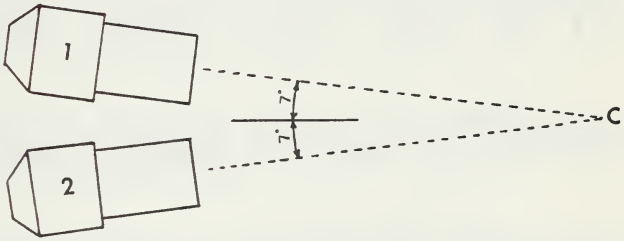

SECTION A-A

X-ray probe arrangement for simultaneous Temperature/Magnetic Field measurements.

FIGURE 36

LIST OF REFERENCES

1. Beady, J.F., Effects of High-Power Laser Radiation, pp.161-207, Academic Press, 1971.

2. Rose, D.J. and Clark, M., Plasma and Controlled Fusion, p.228-236, MIT Press and Wiley, 1961.

3. Ekefors, E., "Spectrum in the Extreme Ultraviolet," Physikalische Zeitschrift, V.31, p.737-738, 1930.

4. Robinson, H.A., "Comments on the Spectroscopy in the Far Ultraviolet and Estimation of Temperature and Pressure in a Spark Vacuum," Zeitschrift fur Physik, V.100, p.636-643, 1936.

5. Jahoda, F.C., and others, "Continuum Radiation in the X-ray and Visible Regions from a Magnetically Compressed Plasma(Scylla)," Physical Review, V.119, p.843-856, 1 August 1960.

6. Naval Research Laboratory Report 6541, Calculations Useful in the Determination of Electron Temperature from X-ray Continuum Radiation Emitted from High Temperature Plasmas, by R.C. Elton and A.D. Anderson, pp.36, 31 March 1967.

7. Naval Research Laboratory Report 6738, Determination of Electron Temperatures Between 100eV and 100KeV from X-ray Continuum Radiation in Plasmas, by R.C. Elton, pp. 66, 11 December 1968.

8. Van Paassen, H.L.L., "A Time-Resolved Ross Filter System for Measuring X-ray Spectra in Z-pinch Plasma Focus Devices," The Review of Scientific Instruments, V.42, p.1823-1824, December 1971.

9. Bernstein, M.J., "Simple X-ray Bandpass Filters for Nanosecond Resolution of Plasma Spectra," The Review of Scientific Instruments, V.43, p.1323-1326, September 1972.

10. Johnson, D.J., "An X-ray Spectral Measurement System for Nanosecond Plasmas," Review of Scientific Instruments, V.45, p.191-194, February 1974.

11. Bobin, J.L., and others, "Temperature in Laser Created Deuterium Plasmas," Nuclear Fusion, V.9, p.115-120,

1969.

12. Mallozzi, P.J., and others, "Laser-generated Plasmas as a Source of X-rays for Medical Applications," Journal of Applied Physics, V. 45, p. 1891-1895, April 1974.

13. Whitney, K.G. and Davis, J., "Conversion Efficiencies of Laser to X-ray Energy in C, F, and Al Plasmas," Applied Physics Letters, V.24, p.509-511, 15 May 1974.

14. Lieber, A., and others, "Micro-Channel Plate as a Parallel-Bore Collimator for Soft X-ray Imaging," Nuclear Instruments and Methods, V.125, p.553-556, 1975.

15. Bogen, P., Plasma Diagnostics (edited by W. Lochte-Holtgraven), p.424-477, Wiley, 1968.

16. Key, M.H., and others, "Time Resolved Absolute X-ray Measurements on Laser Produced Plasmas," Applied Physics Letters, V.25, p.335-337, 15 September 1974.

17. Young, F.C., "Measurements of Energetic X-rays from Laser-Produced Plasmas," Physical Review Letters, V. 33, p.747-750, 23 September 1974.

18. Mulser, P., and others, "Plasma Production by Laser," Physics Reports, V.6C, p.189-239, January 1973.

19. Nishikawa, K., "Laser Interaction with Plasmas," Journal of the Japanese Physical Society, V.24, p.1152-1158, May 1968.

20. Shearer, J.W., and others, "Experimental Indications of Plasma Instabilities Induced by Laser Heating," Physical Review A, V.6, p.764-769, August 1972.

21. Beverly, R.E., "Superthermal Ion and X-ray Emission from a Carbon Dioxide TEA Laser-Produced Polyethylene Plasma," Physics Letters, V.44A, p.321-322, 2 July 1973.

22. Waki, M., and others, "Properties of Plasma Produced by High Power Laser," Japanese Journal of Applied Physics, V.11, p.420-421, 1972.

23. Yamanaka, C., and others, "Nonlinear Interaction of Laser Radiation and Plasma," Physics Letters, V.38A,

p.495, March 1972.

24. Dyer, P.E., and others, "X-ray Emission from a Carbon Dioxide Laser Produced Plasma," Applied Physics Letters, V.24, p.316-317, 1 April 1974.

25. McKee, T.L., An Investigation of the Self-Generated Magnetic Fields Associated with a Laser-Produced Plasma, Ph.D. Thesis, Naval Postgraduate School, Monterey, California, December 1972.

26. Bird, R.S., The Pressure Dependence of Spontaneous Magnetic Fields in Laser Produced Plasmas, Ph.D. Thesis, Naval Postgraduate School, Monterey, California, June 1973.

27. Donaldson, T.P., and others, "Electron Temperature and Ionization States in Laser Produced Plasmas," Journal of Physics B, V.6, p.1532, August 1973.

28. Science Applications, Inc. Report SAI-72-548-LJ, Studies in the Physics of X-ray Generation of Laser-Heated Plasmas, By S. Tamor, p.3-17, October 1972.

29. Stratton, T.F., Plasma Diagnostic Techniques (edited by R.E. Huddlestone and S.L. Leonard), p.359-397, Academic Press, 1965.

30. Davis, I.J, Self-Generated Magnetic Fields Produced by Laser Bombardment of a Solid Target, MS Thesis, Naval Postgraduate School, Monterey, California, June 1971.

31. Callahan, D.J., Laser Plasma Particle Velocities, MS Thesis, Naval Postgraduate School, Monterey, California, June 1976.

32. Quantum Radiation Instruments and Technology (Quantrad) Corporation, 2261 South Carmelina Avenue, Los Angeles, California 90064.

33. Goulding, F.S., "Semiconductor Detectors for Nuclear Spectrometry. I," Nuclear Instruments and Methods, V.43, p.1-54, 1966.

34. Kawecki Berilco Industries (KBI), Inc., Reading, Pennsylvania 19603.

35. Williamson, F.T., Jr., Laser Generated Magnetic Fields,

MS Thesis, Naval Postgraduate School, Monterey, California, June 1976.

36. Dow Chemical (Rocky Flats Division) Report RFP-2174, Chemical Milling of Beryllium for Machining Damage Removal, by R.L. Riegel, E.L. Childs, and K.R. Scully, p.2, 8 July 1974.

37. Buchl, K., and others, Laser Interaction and Related Plasma Phenomena Volume 2 (edited by H.J. Schwarz and H. Hora), p.508, Plenum Press, 1972.

BIBLIOGRAPHY

Ahmed, N. and Key, M.H., "Plasma Temperature in Laser Pulse Induced Gas Breakdown," Journal of Physics B, V.5, p.866-877, 17 November 1971.

Alikaev, V.V., and others, "Measurements of the Plasma Electron Temperature from the Bremsstrahlung Spectrum in the X-ray Region," Recent Advances in Plasma Diagnostics, V.1, p.55-60, 1965.

Baird, D.C., Experimentation: An Introduction to Measurement Theory and Experimental Design, Prentice-Hall, 1962.

Basov, N.G., and others, "Measurement of the Time Variation of the Temperature of the Plasma of a Laser Flare by Means of Its X-radiation," JETP Letters, V.9, p.315-317, 5 May 1969.

Beers, Y., Introduction to the Theory of Error, Addison-Wesley, 1957.

Bekefi, G., Radiation Processes in Plasmas, Wiley, 1966.

Bernstein, E.J. and Hai, F., "An X-ray Pinhole Camera With Nanosecond Resolution," Review of Scientific Instruments, V.41, p.1843-1845, December 1970.

Bernstein, E.J., "Simple X-ray Bandpass Filters for Nanosecond Resolution of Plasma Spectra," The Review of Scientific Instruments, V.43, p.1323-1326, September 1972.

Bertolini, G. and Coche, A., eds. Semiconductor Detectors, Elsevier Publishing Company, 1968.

Beverly, R.E., "Superthermal Ion and X-ray Emission from a Carbon Dioxide TEA Laser-Produced Polyethylene Plasma," Physics Letters, V.44A, p.321-322, 2 July 1973.

Bird, R.S., The Pressure Dependence of Spontaneous Magnetic Fields in Laser Produced Plasmas, Ph.D. Thesis, Naval Postgraduate School, Monterey, California, June 1973.

Birks, J.B., The Theory and Practice of Scintillation

Counting, Pergamon Press, 1964.

Bobin, J.L., and others, "X-rays from a Laser Created Deuturium Plasma," Physics Letters, V.28A, p.396-399, 30 December 1968.

Bobin, J.L., and others, "Temperature in Laser Created Deuturium Plasmas," Nuclear Fusion, V.9, p.115-120, 1969.

Brown, J.G., X-rays and Their Applications, Plenum Press, 1966.

Brukhnevitch, J.F. and Glibert, K.M., "Spectral Analysis of X-rays from Laser-Generated Plasmas," Advances in X-ray Analysis, V.18, p.159-168, 1974.

Buchl, K., and others, Laser Interaction and Related Plasma Phenomena Volume 2 (edited by H.J. Schwarz and H. Hora), p.503-514, Plenum Press, 1972.

Callahan, D.J., Laser Plasma Particle Velocities, MS Thesis, Naval Postgraduate School, Monterey, California, June 1976.

Campbell, J.I. and McNelles, L.A., "An Inter-Comparison of Efficiency Calibration Techniques for Semiconductor X-ray Detectors," Nuclear Instruments and Methods, V.125, p.205-223, 1975.

Campbell, P.M., and others, "Laser-Droven Compression of Glass Microspheres," Physical Review Letters, V.34, p.74-77, 13 January 1975.

Chase, B.C., and Silk, J.K., "Ellipsoid-Hyperboloid X-ray Imaging Instrument for Laser-Pellet Diagnostics," Applied Optics, V.14, p.2096-2098, September 1975.

Chen, F.F., Introduction to Plasma Physics, Plenum Press, 1974.

Colombant, D. and Tonon, G.F., "X-ray Emission in Laser-Produced Plasmas," Journal of Applied Physics, V.44, p.3524-3537, August 1973.

Compton, A.H. and Allison, S.K., X-rays in Theory and Experiment, D. Van Nostrand company, 1934

Cuderman, J.F. and Glibert, K.M., "An X-ray Spectrometer for Laser-Induced Plasma," Review of Scientific Instruments, V.46, p.53-57, January 1975.

Daiber, J.W. and Thompson, H.M., "X-ray Temperatures From Laser-Induced Breakdwon Plasmas in Air," Journal of Applied Physics, V.41, p.2043-2047, April 1970.

Danish Atomic Energy Commission Research Establishment Riso Report 18, International Summer Course in Plasma Physics 1960, edited by C.F. Wandel, November 1960.

Davis, L.J., Self-Generated Magnetic Fields Produced by Laser Bombardment of a Solid Target, MS Thesis, Naval Postgraduate School, Monterey, California, June 1971.

DeMichelis, C. and Ramsden, S.A., "Plasma Production By Laser Beam Irradiation of a Single Solid Particle," Physics letters, V.25A, p.162-163, 31 July 1967.

Dick, K. and Pepin, H., "Nonlinear Interaction of Carbon Dioxide Laser Radiation with Aluminum and Polyethylene Targets," Optics Communications, V.13, p.289-293, March 1975.

Donaldson, T.P., and others, "Electron Temperature and Ionization States in Laser Produced Plasmas," Journal of Physics B, V.6, p.1532, August 1973.

Drake, J.F., "Parametric Instabilities of Electromagnetic Waves in Plasmas," The Physics of Fluids, V.17, p.778-785, April 1974.

Dyer, P.E., and others, "X-ray Emission from a Carbon Dioxide Laser Produced Plasma," Applied Physics Letters, V.24, p.316-317, 1 april 1974.

Ekefors, F., "Spectrum in the Extreme Ultraviolet," Physikalische Zeitschrift, V.31, p.737-738, 1930.

Eliseenko, I.G., and others, "Quantum Yields of the Surface X-ray Photoeffect at 1-10 Angstroms," Soviet Physics - Technical Physics, V.13, p.122-129, July 1968.

Elion, H.A. and Stewart, D.C, eds. Analytical Chemistry: Handbook of X-ray and Microprobe Data, V.9, Pergamon Press, 1969.

Elton, R.C. and Roth, N.V., "Plasma Spectroscopy in the Vacuum Ultraviolet and Soft X-ray Regions," Applied Optics, V.6, p.2071-2078, December 1967.

Evans, R.D., The Atomic Nucleus, McGraw-Hill, 1955.

Floux, F., and others, "X-ray Emission form Laser Created Plasmas," Physics Letters, V.45A, p.483-484, 5 November 1973.

Fowles, G.R., Introduction to Modern Optics, Holt, Rinehart and Winston, 1975.

Fraley, G.S. and Mason, R.J., "Preheat Effects on Microballoon Laser-Fusion Implosions," Physical Review Letters, V.35, p.520-523, 25 August 1975.

Galati, M. and Peacock, H.J., X-ray Spectroscopy of the Ion Population in the Plasma Produced at the Surface of a Plane Massive Target by Intense Laser Irradiation, paper presented at the Sixth European Conference on Controlled Fusion and Plasma Physics, Moscow, USSR, 30 July 1973.

Gaunt, J.A., "Continuous Absorption," Philisophical Transactions of the Royal Society, V.229A, p.163-204, 1930.

Gilbert, K.M., Sandia Laboratory, Albuquerque, N.M., private communication with, 8 December 1975, Subj: light screening for PIN diodes.

Goto, S., and others, "Inverse Bermsstrahlung Process in Plasma Heating," Progresses in Theoretical Physics, V.45, p.1342-1344, 1971.

Gottfreid, B.S., Programming with Fortran IV, Quantum Publishers, 1972.

Goulding, F.S., "Semiconductor Detectors for Nuclear Spectrometry. I," Nuclear Instruments and Methods, V.43, p.1-54, 1966.

Griem, H.R., and others, "Bremsstrahlung from Dense Plasmas," Physics Review Letters, V.2, p.281-282, 1 April 1959.

Griem, H.R., Plasma Spectroscopy, McGraw-Hill, 1964.

Hahlfelder, J.J. and Palmer, M.A., A Pinhole Camera for Photographing X-rays from Laser Produced Plasmas, Sandia Laboratories, Albuquerque, New Mexico, 1975.

Halliday, F.C., and others, Preparation and Use of K-edge and L-edge X-ray Foil Filters, Stanford Research Institute, Menlo Park, California, 1966.

Halverson, W., "Bremsstrahlung Photon Emission Rate from Maxwellian Plasmas," Plasma Physics, V.14, p.601-604, 1972.

Handbook of Military Infrared Technology, Office of Naval Research, 1965.

Hecht, E. and Zajac, A., Optics, Addison-Wesley, 1974.

Huddlestone, R.H. and Leonard, S.L., eds. Plasma Diagnostic Techniques, Academic Press, 1965.

Hudson, R.D., Jr., Infrared Systems Engineering, Wiley, 1969.

Jahoda, F.C., and others, "Continuum Radiation in the X-ray and Visible Regions from a Magnetically Compressed Plasma(Scylla)," Physical Review, V.119, p.843-856, 1 August 1960.

Johnson, D.J., "An X-ray Spectral Measurement System for Nanosecond Plasmas," Review of Scientific Instruments, V.45, p.191-194, February 1974.

Kaelble, E.F., ed. Handbook of X-rays, McGraw-Hill, 1967.

Kas'yanov, Y.S., and others, "Investigation of Laser-Plasma Emission in the X-ray Band," JETP Letters, V.20, p.333-334, 5 December 1974.

Kawashima, N. and Yamobi, A., "Direct Display of Plasma Density and Temperature," Journal of Applied Physics, V.42, p.5400-5403, December 1971.

Kephart, J.F., and others, "Bremsstrahlung Emission from Laser-Produced Plasmas," Applied Physics Letters, V.25,

p.108-109, 15 July 1974.

Key, M.H., and others, "Space Resolved X-ray Measurements on Laser Produced Plasmas," Physics Letters, V.48A, p.121-122, 3 June 1974.

Key, M.H., and others, "Time Resolved Absolute X-ray Measurements on Laser Produced Plasmas," Applied Physics Letters, V.25, p.335-337, 15 September 1974.

Key, M.H., "Measurement of Non-thermal Electron Energy Distributions in High Temperature Laser Produced Plasmas," Journal of Physics B, V.8, p.674-683, 1975.

Klein, E., and others, Variation of the Temperature of Laser-Produced Plasmas with Laser Pulse and Target Parameters, paper presented at the Sixth European Conference on Controlled Fusion and Plasma Physics, Moscow, USSR, 30 July 1973.

Krokhin, O.N., and others, "Anisotropy of X-rays from a Laser Plasma," JETP Letters, V.20, p.105-107, 20 August 1974.

Lee, T.N. and Nagel, D.J., "X-ray Emission from Laser-Produced Magnesium Plasmas," Journal of Applied Physics, V.46, p.3784-3788, September 1975.

Lieber, A., and others, "Micro-Channel Plate as a Parallel-Bore Collimator for Soft X-ray Imaging," Nuclear Instruments and Methods, V.125, p.553-556, 1975.

Lockheed Palo Alto Research Laboratory Report DNA-3404F, X-ray Diagnostics for Laser Systems, by I.F. Case, and others, April 1974.

Locte-Holtgreven, W., ed. Plasma Diagnostics, Wiley, 1968.

Lorrain, P. and Corson, D.R., Electromagnetic Fields and Waves, W.H. Freeman and Company, 1970.

Mallozzi, P.J., and others, "Laser-generated Plasmas as a Source of X-rays for Medical Applications," Journal of Applied Physics, V.45, p.1891-1895, April 1974.

Mandel'shtam, S.L., and others, "Investigation of the Spark Discharge Produced in Air by Focusing Laser Radiation. II," Soviet Physics JETP, V.22, p.91-96, January 1966.

Marion, J.B., Classical Electromagnetic Raditaion, Academic Press, 1974.

Marr, G.V., Plasma Spectroscopy, Elsevier Publishing Company, 1968.

Martineau, J., and others, "Parametric Study of Laser Created Plasmas from Solid Targets," IEEE Journal of Quantum Electronics, V.8, p.551, June 1972.

Mathematical Sciences Northwest Incorporated Report DNA-3251F, Laser Heating of Magnetically Confined Plasmas for X-ray Production, by A.L. Hoffman, November 1973.

McKee, I.L., An Investigation of the Self-Generated Magnetic Fields Associated with a Laser-Produced Plasma, Ph.D. Thesis, Naval Postgraduate School, Monterey, California, December 1972.

Mead, S.W., and others, "Preliminary Measurements of X-ray and Neutron Emission from Laser-Produced Plasmas," Applied Optics, V.11, p.345-352, February 1972.

Moll, J.I., Physics of Semiconductors, McGraw-Hill, 1964.

Mori, C. and Watanbe, T., "Photoelectric Emission of Metals by X-rays in the KeV Region," Japanese Journal of Applied Physics, V.9, p.666-672, June 1973.

Muller, E.W. and Green, T.S., "X-ray Temperature Measurements of Laser Production Plasmas," Plasma Physics, V.13, p.73-75, 1971.

Mulser, P., and others, "Plasma Production by Laser," Physics Reports, V.6C, p.189-239, January 1973.

Murphy, J.A., ed. Surface Preparation and Finishes for Metals, McGraw-Hill, 1971.

Nagel, D.J., and others, "X-ray Emission from Laser-Produced Plasmas," Physical Review Letters, V.33, p.743-746, 23 September 1974.

Naval Research Laboratory Report 6541, Calaculations Useful in the Determination of Electron Temperature from X-ray Continuum Radiation Emitted from High Temperature

Plasmas, by R.C. Elton and A.D. Anderson, 31 March 1967.

Naval Research Laboratory Report 6738, Determination of Electron Temperatures Between 50eV and 100KeV from X-ray Continuum Radiation in Plasmas, by R.C. Elton, 11 December 1968.

Naval Research Laboratory MR-2556, Radiation Escape from an Optically Thick Plasma, by P.S. Julienne and J. Davis, February 1973.

Naval Research Laboratory Report MR-2644, K-shell Line Radiation from Laser-Produced Aluminum Plasmas, by K. Whitney, J. Davis and E. Oran, June 1973.

Naval Research Laboratory Report 7728, Response of Materials to Laser Radiation: A Short Course, by J.T. Schriempf, 10 July 1974.

Nishikawa, K., "Parametric Excitation of Coupled Waves. I. General Formulation," Journal of the Physical Society of Japan, V.24, p.916-1152, April 1968.

Nishikawa, K., "Laser Interaction with Plasmas," Journal of the Japanese Physical Society, V.24, p.1152-1158, May 1968.

Nishikawa, K., "Parametric Excitation of Coupled Waves. II. Parametric Plasmon-Photon Interaction," Journal of the Physical Society of Japan, V.24, p.1152-1158, May 1968.

Nuckolls, J., and others, "Laser-Induced Thermonuclear Fusion," Physics Today, p.46-53, August 1973.

Paresce, F., "Quantum Efficiency of a Channel Electron Multiplier in the Far Ultraviolet," Applied Optics, V.14, p.2823-2824, December 1975.

Pieroni, L. and Segre, S.E., "Observation of Non-Maxwellian Electron Distribution Functions in the Alcator Device by Means of Thomson Scattering and Their Interpretation," Physical Review Letters, V.54, p.928-930, 14 April 1975.

Podgornyi, I.M., Topics in Plasma Diagnostics, Plenum Press, 1971.

Puell, H., and others, "Time Resolved Temperature Measurements of a Laser Produced Carbon Plasma," Physics

Letters, V.37A, p.35-36, 25 October 1971.

Rager,J.P. and Robouch, B.V., "Applicability of X-ray Filter Method to Thermometry of a Ncncorona $(CH_2)n$ Laser-Produced Plasma," Applied Physics Letters, V.26, p.664-665, 15 June 1975.

Ready, J.F., Effects of High-Power Laser Radiation, pp.161-207, Academic Press, 1971.

Richtmeyer, F.K., Kennard, E.H and Cooper, J.N., Introduction to Modern Physics, McGraw-Hill, 1969.

Ripin, B.H., and others, "X-ray Emission Spectra from High-Power-Laser-Produced Plasmas," Physical Review Letters, V.34, p.1313-1316, 26 May 1975.

Robinson, H.A., "Comments on the Spectroscopy in the Far Ultraviolet and Estimation of Temperature and Pressure in a Spark Vacuum," Zeitschrift fur Physik, V.100, p.636-643, 1936.

Rose, D.J. and Clark, M., Plasma and Controlled Fusion, MIT Press and Wiley, 1961.

Rumsby, P.T. and Paul, J.W., "Temperature and Density of an Expanding Laser Produced Plasma," Plasma Physics, V.16, p.247-260, 1974.

Schwarz, H.J. and Hora, H., eds.Laser Interaction and Related Plasma Phenomena, V.2, Plenum Press, 1972.

Schwarz, H.J. and Hora, H., eds.Laser Interaction and Related Plasma Phenomena, V.3A and 3B, Plenum Press, 1974.

Schwob, J.L. and Fraenkel, B.S., "Evidence for High Temperatures in Minute Plasma Points from X-ray Spectra of FeXXV and FeXXVI," Physics Letters, V.40A, p.81-82, 19 June 1972.

Science Applications, Inc. Report SAI-72-548-LJ, Studies in the Physics of X-ray Generation of Laser-Heated Plasmas, by S. Tamor, p.3-17, October 1972.

Sears, F.W. and Salinger, G.L., Thermodynamics, Kinetic Theory, and Statistical Thermodynamics, Addison-Wesley, 1975.

Segre, S.E. and Pieroni, L., "Measurement of Non-Maxwellian Electron Distribution Functions in Hot Plasma and the Importance for Thomson Scattering Diagnostics," Physics Letters, V.51A, p.25-26, 27 January 1975.

Shampine, L.F., and Allen, R.C., Jr., Numerical Computing: An Introduction, W.B. Saunders Company, 1973.

Sharpe, J., Nuclear Radiation Measurement, Temple Press, 1960.

Shatas, E.A., "Soft X-rays from a Laser-Heated Dense Plasma Focus," Journal of Applied Physics, V.42, p.5884-5886, December 1971.

Shearer, J.W., and others, "Experimental Indications of Plasma Instabilities Induced by Laser Heating," Physical Review A, V.6, p.764-769, August 1972.

Smith, W.V., Laser Applications, Artech House, 1970.

Spitzer, L., Jr., Physics of Fully Ionized Gasses, number 3, Wiley, 1962.

Stumpfel, C.R., and others, "Investigation of the Early Phases of Plasma Production by Laser Irradiation of Plane Solid Targets," Journal of Applied Physics, V.43, p.902-907, March 1972.

Sze, S.M., Fysics of Semiconductor Devices, Wiley, 1969.

Thomson, W.L., and others, "Parametric Instability Thresholds and Their Control," The Physics of Fluids, V.17, p.849-851, April 1974.

Van Paassen, H.L.L., "A Time-Resolved Bcss Filter System for Measuring X-ray Specta in Z-pinch Plasma Focus Devices," The Review of Scientific Instruments, V.42, p.1823-1824, December 1971.

Vclyak, T.B., and others, "Effect of Magnetic Field on Soft X-ray Radiation from Laser Plasma," Soviet Physics JETP,

V.37, p.245-246, August 1973.

Waki, M., and others, "Properties of Plasma Produced by High Power Laser," Japanese Journal of Applied Physics, V.11, p.420-421, 1972.

Weast, R.C., ed. CRC Handbook of Chemistry and Physics, 54th edition, Chemical Rubber Publishing Company, 1973.

Whitlock, R.R., Naval Research Laboratory, private communication with, 2 December 1975, Subj: use of PIN diodes and absorption filters in the vicinity of a laser plasma.

Whitney, K.G. and Davis, J., "Conversion Efficiencies of Laser to X-ray Energy In C, F, and Al Plasmas," Applied Physics Letters, V.24, p.509-511, 15 May 1974.

Willardson, R.K. and Beer, A.C., eds. Semiconductors and Semimetals, V.7B, Academic Press, 1971.

Williamson, F.T., Jr., Laser Generated Magnetic Fields, MS Thesis, Naval Postgraduate School, Monterey, California, June 1976.

Wright, E.L. and Bekefi, B., "Radiation Temperature of a Bounded Nonthermal Plasma: II Experiment," The Physics of Fluids, V.14, p.1773-1781, August 1971.

Yamabe, C., and others, "Interaction of TEA Carbon Dioxide Laser Light with Plasma," Physics Letters, V.50A, p.349-350, 30 December 1974.

Yamanaka, C., and others, "Nonlinear Interaction of Laser Radiation and Plasma," Physics Letters, V.38A, p.495, March 1972.

Yariv, A., Introduction to Optical Electronics, Holt, Rinehart and Winston, 1971.

Young, F.C., "Measurements of Energetic X-rays from Laser-Produced Plasmas," Physical Review Letters, V.33, p.747-750, 23 September 1974.

Young, H.D., Statistical Treatment of Experimental Data, McGraw-Hill, 1962.

INITIAL DISTRIBUTION LIST

		No. Copies
1.	Defence Documentation Center Cameron Station Alexandria, Virginia 22314	2
2.	Library, Code 0212 Naval Postgraduate School Monterey, California 93940	2
3.	Department chairman, Code 61Wh Department of Physics and Chemistry Naval Postgraduate School Monterey, California 93940	2
4.	Professor A.W. Cooper, Code 61Cr (thesis adv) Department of Physics and Chemistry Naval Postgraduate School Monterey, California 93940	3
5.	Assoc Prof F.R. Schwirzke, Code 61Sw (thesis adv) Department of Physics and Chemistry Naval Postgraduate School Monterey, California 93940	1
6.	Captain S.A. Shewchuk, CF (student) National Defence Headquarters DGAMMC/DAME 3 Ottawa, Ontario, Canada K1A 0K2	2